A Survey of Coastal Conditions around the Continental US Using a High-Resolution Ocean Reanalysis

Michael A. Alexander[1], James D. Scott[1,2], Michael G. Jacox[1,3,4], Clara Deser[5], Dillon J. Amaya[1], Antonietta Capotondi[1,2], Adam S. Phillips[5]

[1] NOAA Physical Sciences Laboratory, Boulder CO, USA
[2] CIRES, University of Colorado, Boulder, CO USA
[3] NOAA Southwest Fisheries Science Center, Monterey, CA, USA
[4] University of California Santa Cruz, Santa Cruz, CA, USA
[5] National Center for Atmospheric Research, Boulder, CO, USA

Key words:
Coastal Oceanography; US Continental Shelves; Ocean Reanalysis; Temperature Salinity; Mixed Layer Depth

Corresponding Author:
Michael Alexander
NOAA/Physical Sciences Laboratory
325 Broadway
Boulder, CO 80305
michael.alexander@noaa.gov

Abstract

Obtaining a long-term perspective on the evolution of the ocean is hindered by a lack of sub-surface observations. Ocean reanalyses, which merge fields from an ocean model with observations using complex data assimilation techniques, provide a dynamically consistent estimate of the ocean in time and space. Recently developed ocean reanalyses, several with resolutions finer than 10 km, provide a three-dimensional view of the ocean, including on the continental shelf. Here, we use monthly fields from the 1/12° Global Ocean Reanalysis and Simulations (GLORYS) over the years 1993-2019 to provide a broad survey of temperature, salinity, and mixed layer depth over the shelf (depth < 400 m) around the continental United States. The analyses reveal noteworthy aspects of the coastal oceanography, including: i) how bathymetry shapes the seasonal cycle of bottom water temperature (BWT) and the role of the mixed layer in linking the BWT and sea surface temperature (SST) anomalies; ii) the persistence, trends and distributions of SST and BWT anomalies, which strongly influence extremes such as marine heatwaves; iii) the influence of the outflow from the Mississippi and Columbia rivers on the adjacent ocean; and iv) how the mean and anomalous vertical structure of temperature and salinity vary between the northeast, southeast, Gulf of Mexico and California Current Large Marine Ecosystems. In addition to documenting coastal ocean conditions, the broader goal of the survey is to encourage more detailed studies using high resolution ocean reanalyses such as GLORYS.

Introduction

The coastal ocean, ranging from the shore to the outer edge of the continental shelf, is influenced by the depth and shape of the seafloor and by a wide array of physical processes. For example, ocean conditions around the continental United States are strongly influenced by: the proximity of the Gulf Stream and Labrador current, combined with an array of bays, banks and basins along the east coast, the wide West Florida Shelf (WFS); outflow from the Mississippi River in the Gulf of Mexico (GOMEX)and wind-driven upwelling over the steep and narrow shelf on the west coast. In addition, the continental margins provide critical habitat for marine ecosystems and for economic activity including tourism, aquaculture and fishing. Commercial and recreational saltwater fishing generated over $255 billion in sales impacts, contributed $117 billion to gross domestic product, and supported 1.8 million jobs in the U.S. in 2019 (National Marine Fisheries Service, 2022), where the majority of the catch occurred on the shelf.

Temperature, salinity and mixed layer depth are key components of ocean physics that also strongly regulate the biogeochemistry and ecology of the coastal ocean. Temperature influences physiological processes in marine organisms (Fry, 1971; Rivkin and Legendre, 2001; Deutsch et al., 2015). Surface temperatures modulate air-sea interactions and are often an indicator and/or driver of marine ecosystem fluctuations (Mueter et al., 2009; Drinkwater et al., 2010; Ottersen et al., 2010), including fish distributions (e.g., Nye et al., 2009; Block et al., 2011; Pinsky et al., 2013), fish recruitment (e.g., Planque and Fredou, 1999; Hunt et al., 2011; Kristiansen et al., 2011) and biodiversity (Edwards and Richardson, 2004; Tittensor et al., 2010). Bottom water temperature is critical to benthic organisms, including bivalves (Barber and Blake, 2006) and demersal fish species (Harvey, 2009; Younes et al., 2020). Salinity, including shelf bottom waters, can also influence marine species (Hedger et al., 2004; Miller et al., 2016). Salinity is also an important characteristic of water masses (e.g., Tomczak, 1999; Liu and Tanhua, 2021), it influences uptake of CO_2 by the ocean, and has been used to estimate alkalinity and other biogeochemical variables (Cai et al., 2010; Salisbury and Jönsson, 2018; Carter et al., 2021). The distribution of both temperature and salinity controls the density profile and thus static stability and vertical mixing. The mixed layer depth (MLD) also varies due to the surface buoyancy and wind forcing and by dynamic ocean processes including upwelling, eddies and fronts (Fox-

Kemper et al., 2022). The MLD affects the availability of nutrients for phytoplankton and marine plants and the time phytoplankton remain in the euphotic zone in light limited regions. Long term changes in temperature, salinity and MLD (Jang et al., 2011; Alexander et al., 2018; Cheng et al., 2020; Fox-Kemper et al., 2021) as well as sea level rise, ocean acidification, and deoxygenation due to increasing greenhouse gasses are already impacting coastal marine ecosystems and these changes are likely to become more pronounced in the future (Scavia et al., 2002; He and Sillman., 2019).

Long-term measurements provided by buoys, surface stations, trawl surveys and sampling programs such as CalCOFI (Bograd et al., 2003) off Southern California and the Oleander survey line (Rossby and Gotlieb, 1998) between New Jersey and Bermuda have provided information about regional coastal conditions, including temperature, salinity and MLD. Measurements of surface conditions from satellites and the advent of profiling floats and unmanned vehicles have greatly enhanced our ability to observe the ocean (e.g., Legaard and Thomas, 2006; Rudnick, 2016; Roemmich et al., 2019; Erichsen and Middelboe, 2022). Despite recent advances in monitoring the ocean, *in situ* observations are still very limited in space and time, while satellites only measure the ocean surface and have difficulty measuring some variables in near-shore regions. In contrast to sea surface temperature (SST), measurements of bottom water temperature (BWT) are very limited, as there are few long time series of near bottom conditions on the shelf, and measurements from trawl surveys are scattered in space and infrequent in time. In addition, measurements of salinity throughout the water column are much more limited than those for temperature. Estimating MLD depends on collocated vertical temperature and salinity profiles, which can be obtained from ARGO floats since around 2004 but are still relatively sparse, especially in coastal areas.

Atmospheric reanalyses were first developed more than 25 years ago (Kalnay et al., 1996) to provide a physically-consistent and continuous record of conditions throughout the atmospheric column. They are based on prediction systems that assimilate observations and merge them with a first guess field provided by the model to initialize a forecast. In a reanalysis, this procedure is repeated at set intervals to generate a continuous record in time and space, using the same model throughout the process. Using a similar method, ocean reanalyses were developed beginning in

the late 1990s (Carton et al. 2000). Ocean reanalyses are driven by surface atmospheric conditions, often provided by an atmospheric reanalysis, and assimilate *in situ* observations and measurements from satellites. Until very recently, ocean reanalyses had fairly coarse horizontal resolution (~1°; ~100 km) adequate for resolving large-scale phenomena, such as the El Niño/Southern Oscillation, but not mesoscale processes. Improvements in model physics, data assimilation techniques and the ocean observing system have all contributed to advance ocean reanalyses (e.g., see Moore et al., 2019, Storto et al., 2019). With horizontal resolutions of 10 km or finer and more than 40 vertical levels, ocean reanalyses are now capable of resolving coastal processes.

Ocean reanalyses can be regional or global. An example of the former is the reanalysis of the California Current System (Neveu et al., 2016), which has provided key input in several applications (Becker et al., 2016; Tolimieri et al., 2018; Haltuch et al., 2020), although some biases have been noted (Schroeder et al., 2014; Amaya et al., 2023a). Recently, fine resolution global reanalyses including the Global Ocean Reanalysis and Simulations (GLORYS, V12; Lellouche et al., 2021), Blue Link Reanalysis (BRAN, Chamberlain et al. 2021) and the Hybrid Coordinate Ocean Model (HYCOM, https://www.hycom.org/reanalysis) have been developed. However, global reanalyses were not specifically developed to represent regional coastal features, raising the question: how well do they depict actual conditions? De Souza et al. (2021) examined ocean conditions in the vicinity of New Zealand and found that the GLORYS reanalysis performed well, with more realistic variability and relatively small biases in the water column structure compared to other reanalyses. However, all simulations had some biases and coastal currents were not well represented. Russo et al. (2022) found that GLORYS, BRAN and HYCOM simulated southern Africa's major oceanographic features reasonably well; GLORYS was deemed to be the most accurate reanalysis for many quantities but overestimated the MLD.

Recent studies have also been undertaken using reanalyses in US coastal regions. Analyses of conditions on the northeast US continental shelf also indicated that monthly SST anomalies from GLORYS were highly correlated ($r > 0.96$) with observations (Chen et al., 2021), and that MLD was represented reasonably well in terms of its seasonal cycle as well as its interannual variability ($r = 0.5–0.8$) (Cai et al., 2021). Castillo-Trujillo et al. (2023) evaluated eight ocean

reanalyses on the northeast US shelf by comparing them to several different data sources for temperature, salinity and sea surface height. They found that higher resolution reanalyses (1/10˚ or finer) performed better than coarser ones (¼˚ or coarser), and GLORYS and HYCOM were identified as the most accurate reanalysis for the metrics evaluated. (Amaya et al., 2023a&b) found that GLORYS represented nearshore ocean parameters such as coastal sea level and bottom temperature along the US west coast continental shelf reasonably well. It also accurately depicted coastally trapped waves that propagate poleward along the west coast of North America, as verified against tide gauge data (Amaya et al., 2022). However, GLORYS slightly overestimated SST variability, and in GLORYS and the other reanalyses examined, sea surface salinity was less accurate than temperature, particularly near the outflow of the Columbia River (Amaya et al. 2023a).

Here we take the opportunity afforded by a powerful new resource – a global high-resolution ocean reanalysis – to do a comprehensive baseline assessment of physical variability over the continental US shelf. We chose to use the GLORYS reanalysis because it has the highest resolution of current global reanalyses and its overall high-level of skill based on multiple assessments. We examine temperature, salinity and MLD over the shelf (< 400 m bottom depth) around the Continental United States (CONUS), including the mean seasonal cycle, as well as the variability, as characterized by the persistence, standard deviation, skewness, kurtosis and histograms of monthly anomalies. Skewness and kurtosis have been shown to be important components of SST variability over portions of the global oceans (Sura and Sardeshmukh, 2008) and skewed or heavy tailed distributions can complicate evaluating the effects of global warming on climate extremes (Sardeshmukh et al., 2015). We examine aspects of the coastal oceanography, including how bathymetry and mixed layer depth affect BWTs and their relationship to SSTs; the influence of the Mississippi and Columbia river discharge on the Gulf of Mexico and the Pacific coastal waters, respectively, and the vertical structure of temperature and salinity around the continental US.

Data and Methods

GLORYS Reanalysis

Here we analyze monthly fields from the GLORYS 1/12˚ (~9 km horizontal resolution) global Mercator Ocean and sea ice reanalysis (Lellouche et al., 2021) from the Copernicus Marine Environmental Monitoring Service (CMEMS). It has 50 vertical levels, with 22 levels in the upper 100m. The near-surface layers have a vertical resolution of 1 m with the layer thickness increasing with depth, reaching 450 m at 5,000 m. The reanalysis uses the Nucleus for European Modeling of the Ocean (NEMO) platform (Madec et al., 2008), forced at the surface by the European Center for Medium-Range Weather Forecasts (ECMWF) ERA-Interim atmospheric reanalysis (Dee et al., 2011). The model assimilates along-track satellite altimetry for the sea surface height, satellite sea surface temperature (SST), sea ice concentrations, and in situ profiles of temperature and salinity, including ARGO floats, from the Coriolis Ocean database ReAnalysis (CORA) dataset (Szekely et al., 2019). Ocean observations are assimilated by means of a reduced-order Kalman filter. A bias correction is applied to the surface radiation and precipitation, while a 3D-VAR scheme is also applied to correct for slowly-evolving large-scale biases in temperature and salinity. The reanalysis extends from 1993 to 2019.

We compute MLD values based on the depth at which the density exceeds that at the surface by 0.125 kg m^{-3}, using daily temperature and salinity profiles and then averaging the daily MLD to obtain monthly values. This criterion was used by Monterey and Levitus (1997), Alexander et al. (2018) and Buckley et al. (2019), but is a larger density difference than has been used in some analyses (e.g., de Boyer Montegut, 2004; Cai et al., 2021). MLD is also provided as a standard output with the GLORYS reanalysis, calculated using a density jump corresponding to a temperature change of 0.2°C with a minimum MLD value set to 10m, which resulted in many locations having this fixed value during summer months. We chose to calculate MLD using the larger density jump as it is generally deeper than 10m, is more representative of the seasonal evolution of the MLD, and reduces large daily fluctuations in MLD.

Results are presented for the coastal waters adjacent to the continental United States and the Atlantic Maritime provinces in Canada, the entire Gulf of Mexico, the northwest portion of the Caribbean, and the Gulf of California (Fig. 1). Maps for winter (January-February-March, JFM) and summer (July-August-September, JAS) are presented for the full domain in the main text, while maps for all seasons for three subregions [northeast US (NEUS), southeast US

(SEUS)/Gulf of Mexico (GOMEX) and the California Current System (CCS)] are presented in the supplemental (S). The regional maps provide a more detailed view of coastal conditions, especially along the west coast and in other regions where the continental shelf is very narrow. The NEUS, SEUS, GOMEX and CCS comprise the four major large marine ecosystems (LMEs, outlined in gray in Fig. 1) around CONUS; LMEs are coherent ocean areas generally along continental margins whose bathymetry, hydrography, and ecology are similar (Sherman and Duda, 1999). Regional averages for all four seasons, including spring (April-May-June, AMJ) and fall (October-November-December, OND) are shown in the supplemental. Monthly anomalies (monthly values with the 1993-2019 mean subtracted) are used to analyze variability, except for interannual standard deviations (Figs. 11, 12, 17-20), which are calculated using seasonally averaged anomalies.

Results

Mean climate

The GLORYS long-term mean sea surface temperature (SST), bottom water temperature (BWT; for depths ≤ 400 m) and mixed layer depth (MLD) during winter are shown in Fig. 2. At the surface, cold water (< 10°C) on the continental shelf extends southward along the east coast from Newfoundland to Cape Hatteras in winter. There is a strong gradient near the shelf break (as indicated by the 400 m isobath in Fig. 1), with warmer SSTs over the open ocean. Cool SSTs are found along the SEUS and GOMEX coasts, with warmer water offshore. The Gulf Stream is readily apparent as a narrow band of warm water (> 23°C) off the southeast coast that extends northeastward into the Atlantic. Along the west coast, SSTs progressively increase from Washington state to the tip of Baja California, from about 8 to 22C.

During winter, the bottom water temperature is low (<10°C) for nearly all of the northeast coast with a sharp break at Cape Hatteras (Fig. 2b). BWTs are moderate (~15°C) adjacent to the coast and at the shelf break, but warmer at mid-shelf over most of the SEUS coast and the northern portion of GOMEX; in contrast, temperatures increase towards the coast over the southern part of the Gulf. Bottom temperatures in winter increase southward along the WFS but are colder

along the outer edge of the shelf slope. BWTs are cold along the US west coast and moderate along both coasts of Baja California.

Compared to the open ocean, the MLD in winter is relatively shallow (<50 m) on nearly all of the US continental shelf (Fig. 2c). The mixed layer on the shelf is constrained by the bathymetry in some regions and by processes such as limited mechanical mixing, since wind speeds generally increase offshore. A clear exception is the western and northern portion of the Gulf of Maine (GOMA) and a narrow region around Georges Bank, where a deeper bottom coupled with cold air originating over the continent increases buoyancy mixing (Brown and Beardsley 1978; Mountain and Jessen, 1987), resulting in deeper mixed layers (70-100m). The MLD is also relatively deep (50-75 m) on the outer portion of the WFS. The MLD is influenced by current systems and is relatively shallow (60-75 m) in the vicinity of the Gulf Stream and the northern edge of the loop current in the GOMEX, relative to the adjacent open ocean.

During summer, the climatological SSTs on the NEUS shelf exhibit a monotonic increase southward along the coast, with a very strong zonal gradient at the shelf break east of New England and Canadian Maritime provinces (Fig. 2d). Very warm SSTs (> 28°C) occur over the southern portion of the domain, including the SEUS coast, Gulf Stream region, the entire GOMEX and the Gulf of California. The relatively cool water adjacent to the US west coast is associated with near-shore upwelling, with a broader region of cool water due to equatorward transport by the California Current and offshore advection by Ekman transport and westward propagating eddies (Huyer 1983; Jacox et al. 2014).

Bottom water temperatures remain cold (< 10°C) for most of the NEUS during summer, although they are relatively warm on Georges Bank and adjacent to the coast from Cape Cod to Cape Hatteras (Fig 2e). BWTs are very warm (> 28°C) near the coast in SEUS and GOMEX but cool substantially near the shelf break, as the nearshore waters warm substantially from winter while those offshore remain relatively unchanged. BWTs are cold during summer along the US west coast but warm along most of the eastern side of the Gulf of California.

The MLD is shallow (< 40m) over most of the CONUS shelf throughout the year and is even shallower (< 15m) over the continental shelf in summer (Fig. 2f). The MLD is especially shallow in the vicinity of where the Mississippi River enters the GOMEX in both summer and winter, likely due to the input of fresh, low-density water.

Given the exceptionally narrow shelf along the west coast of North America (the median CCS shelf width is 34 km), we also present Hovmöller diagrams of conditions in the CCS in Fig. 3, where values on the shelf (< 400 m depth) are first zonally averaged and then shown as a function of calendar month and latitude. The mean SST on the shelf (contours in Fig. 3a) ranges from approximately 10 to 20°C over the meridional extent of the domain during Jan-May. Warming occurs in May north of ~40°N reaching ~14°C during summer. The seasonal cycle in SST is very muted between 35° and 40°N, with a slight peak in September, due to strong upwelling of cold water in spring and summer. The seasonal cycle is larger farther south, especially south of 30°N, where temperatures exceed 20°C in September. The BWT remains near 10°C north of 32°N throughout the year, with somewhat higher temperatures during fall and winter south of this latitude (Fig. 3b), off the west coast of Baja California. The mean MLD on the CCS shelf has values generally between 20 and 40 m in winter, with a maximum of ~50m at 46°N in January (Fig. 3e). MLD values drop to ~10 m or less in spring and remain very shallow through summer.

Given the influence of bathymetry on temperature, we show the BWT climatology as a function of bottom depth on the shelf; results are presented in Fig. 4 as box and whisker plots for JFM, MAM, JAS, OND for grid points located in four regions: NEUS, SEUS, GOMEX and the CCS. In the NEUS during winter, the median BWT rises from approximately 5°C for isobaths < 20 m to 9°C at ~360 m with a very slight decrease below that. The spread, as a function of location in the region, is large for bottom depths less than 120 m, where the full range exceeds ~10°C. In some NEUS locations (particularly in the GOMA), the salinity gradient enables the water column to remain stable despite an increase in temperature with depth, especially in winter (e.g., Figs. 5a, b and Fig. 17). The BWT in the upper 40 m warms in spring and especially during summer, as heating from the surface is mixed to the bottom where the shelf is shallow. The seasonal increase in temperature is more modest for bottom depths between 60 and 140 m from

JFM to JAS. The upper ocean cools in fall, such that BWT decreases monotonically with depth to the 160 m isobath, with temperatures at deeper bottom depths similar to those in the other seasons.

The median SEUS BWT values during JFM increase from ~18°C for points located near the surface to ~20°C between 60 and 100m bottom depths, and decrease at greater depth, although the warmest values (~22°C) in winter are similar throughout the region (Fig. 4b). Bottom temperatures exhibit a monotonic decrease with depth in spring and summer, where BWTs in JAS exceed 28°C near the surface for some locations within SEUS. From summer to fall, BWTs cool substantially for depths less than 40 m but warm slightly between 40-80 m. BWTs decrease with depth below 60m in OND. The temperature range is highly skewed in space, with the warmest locations nearly 10°C warmer than the median and the coldest locations only ~2°C colder than the median. In general, BWTs in the GOMEX are similar to those in the SEUS, except they tend to be slightly warmer and exhibit a much-reduced range at most depths (Fig. 4c, g, k, o).

Temperatures range between 8°C and 20°C with a median of ~12°C for grid points where the bottom is shallower than 20m in the CCS during JFM (Fig. 4d). During winter, the median temperature and temperature range generally decreases slowly with bottom depth to 400 m. This pattern for the CCS generally holds throughout the year, although the near-surface waters are warmer and the range is larger in the other seasons, particularly in summer.

Maps of sea surface salinity indicate that the SSS increases equatorward along the Atlantic coast, ranging from approximately 32 psu to 36 psu from Maine to Florida during JFM (Fig. 5a). Fresher water extends over much of the NEUS shelf but is confined close to the coast in SEUS. High values occur offshore in the Atlantic with slighter lower values in the Caribbean. Low salinity water (< 25 psu) stretches along the central north coast of the GOMEX due to the large input of freshwater by the Mississippi River. A smaller plume of low salinity water also occurs along the narrow shelf off the northwest coast as a result of outflow from the Columbia River and the salinity is slightly lower in the vicinity of San Francisco Bay (~37°N; Fig. 3c & 5a). The bottom and sea surface salinity exhibit similar patterns over most of the continental US shelf, but

with higher salinity at depth. One notable feature visible in the bottom salinity but not surface salinity is in GOMA, where saltier Atlantic water enters the gulf at depth at its southeastern edge via the Northeast Channel.

In general, the summer and winter SSS patterns are similar (Fig. 5), although the inner half of the GOMA is fresher during JAS and the high salinity water in the Northeast Channel is even more prominent in summer. In most regions, the bottom water salinity (BWS) is also similar to its winter counterpart. However, off the northwest coast, the mean SSS is much lower in summer than in winter and is much fresher than the bottom salinity, due to the low-density freshwater output from the Columbia River, which peaks in late spring-early summer (e.g., Helaire et al. 2019).

The timing of the maximum and minimum SSTs and BWTs at each location are shown in Fig. 6. The warmest SSTs generally occur during August in the western Atlantic and GOMEX and in near-shore regions in the northern and southern parts of the domain in the Pacific. The highest SSTs occur during September in the Caribbean and over much of the eastern Pacific including along the coast of California and Baja California. The coldest month for SST is March for most of the north and east portion of the NEUS shelf and February for near shore regions south of Cape Cod. SSTs reach their minimum in February in the Caribbean and Gulf of Mexico, except for a thin strip adjacent to the northern GOMEX coast, where the coldest temperatures occur in January. The month when the coldest SSTs occur is more variable along the west coast: most locations reach a minimum in February or March but there are near shore regions where the lowest value occurs in January and a broader area to the west of southern Baja California where it occurs as late as May.

The month when maximum BWT occurs around the US (Fig. 6b) is much more variable than for SST. The BWT maximum occurs during October or November for most of the NEUS shelf. Surprisingly, the maximum BWT occurs during mid-to-late winter in the deeper portions of central GOMA. Du et al. (2021) attributed the unusual seasonal variation of deep-water temperatures in the GOMA to the timescale of advection of slope water into the Gulf through the Northeast Channel. On the SEUS and northern GOMEX shelves, the month with the highest

BWTs increases with distance from the shore, ranging from Jul-Aug near shore to Oct-Nov offshore at depths of 200-400 m — 2-3 months later than at the surface. Except for a very narrow strip near the shore (also see Fig. S39), the maximum BWTs along the northern ⅔ of the US west coast occur during winter, prior to the start of the upwelling season. Farther south, the maximum occurs in late summer and fall.

The minimum BWTs occur during Feb-Apr in shallower regions of the NEUS shelf and later in deeper areas, especially in GOMA where it can occur in late spring or summer (Fig. 6d). Along the SEUS, WFS and northern GOMEX coasts, the coldest month occurs in the near-shore region in January, and later in the year offshore – in summer or even fall on the edge of the shelf. The coldest month on the west coast is generally in late spring or early summer during the upwelling season.

The months when the deepest and shallowest mixed layer depths occur are shown in Fig. 7. The deepest mixed layers occur from November to February on the northeast continental shelf. In the SEUS and northern GOMEX, the MLD reaches a maximum in October to December, while over deeper waters in the Atlantic and Gulf of Mexico it primarily occurs from January to March. The month with the maximum MLD is highly variable on the narrow west coast shelf ranging from October to February, but occurs during January or February in the open ocean. The shallowest MLDs tend to occur during June or July along the east coast, with isolated areas on the mid-Atlantic and southeast shelves occurring earlier in the year. On the WFS and the northwest portion of GOMEX, the minimum MLD occurs as early as February adjacent to the coast but later in the year, often in June and July, towards the open ocean. The minimum MLD occurs during June through September in the southern GOMEX, except for a very small region on the western side of the Yucatan Peninsula where it occurs early in the year. In the Pacific, the MLD is shallowest in May or June along portions of the US and west coast of Mexico but occurs earlier near San Francisco Bay. In contrast, the minimum MLD occurs during July and August over most of the open ocean in the east Pacific.

The MLD relative to the underlying bathymetry will likely influence how closely conditions at the surface and the bottom, such as SST and BWT, are linked. Thus, we also present the ratio of

the MLD to the bottom depth (in percent) during the deepest and shallowest months in Fig. 7. When the mixed layer is deepest, it reaches at or close to the bottom on the shelf over most of the east coast and GOMEX. The main exception is portions of the GOMA, where the MLD is much shallower than the bottom. This may result from the intrusion of dense water at depth through the Northeast Channel and because much of the gulf is deeper than 150 m with basins that are more than 200 m deep. The MLD/bathymetry ratio is highly variable adjacent to the west coast, but it exceeds 70% between 40° and 45°N. For locations where the mixed layer reaches close to or on the bottom, it can remain there for several months and thus it is more appropriate to consider an extended period with a maximum depth, rather than a single month.

When the MLD is at a minimum, the MLD is generally less than 20% of the bottom depth on the NEUS shelf except in the vicinity of Cape Cod (Fig. 7d). The minimum MLD/bathymetry ratio increases from less than 10% at the shelf break to 50-80% in nearshore regions in SEUS. This gradient is even stronger along the WFS, ranging from < 10% to > 90% from west to east across the shelf. The MLD relative to the bathymetry varies over the remainder of GOMEX where the MLD is very shallow relative to the bottom depth in the northeast and southwest portions of GOMEX, while it exceeds 50% of the bottom depth in the northwest gulf and northwest of the Yucatan Peninsula. The minimum MLD is generally less than 20% of the bottom depth along the west coast.

Interannual Variability

The relationship between surface and bottom temperature anomalies is illustrated in Fig. 8 (top row) by the local concurrent correlation between the two during JFM and JAS. The correlations between SST and BWT are high (> 0.8) over most of the continental shelf along the east and gulf coasts during winter. In most regions, this likely reflects temperature anomalies created at the surface that extend towards the bottom, due to strong wind and buoyancy mixing in winter. In some locations, higher correlations between the two may reflect dynamic ocean processes that influence the entire water column. The JFM SST-BWT correlations are lower (< 0.5) in the center of the GOMA and on the outer edge of the continental shelf on the east and GOMEX coasts. The correlation values are also high along the CCS coastline in JFM but drop offshore as

the shelf deepens rapidly and the MLD is relatively shallow. The SST-BWT correlations remain high adjacent to the CONUS coast in summer but are greatly reduced over much of the continental shelf compared to winter (Fig. 8c, also see Fig. 3f). This is consistent with the shoaling of the mixed layer in spring and shallow MLDs in summer, effectively decoupling the surface from the deeper ocean. The surface and bottom may remain correlated to some degree as temperature anomalies created over the entire water column persist from winter to summer associated with the relatively high auto-correlation of ocean temperature anomalies (see Fig. 10).

The geographical structure of concurrent correlations between surface and bottom salinity anomalies is generally similar to that for temperature, with some notable exceptions (Fig. 8, bottom). These include deeper portions of the shelf along the east coast, where SSS and BWS anomalies are uncorrelated or even exhibit a small negative correlation in both summer and winter. However, during summer, Georges Bank and other shallow regions in the NEUS exhibit higher correlations for SSS-BWS than for SST-BWT. In the GOMEX, the surface and bottom temperature and salinity are uncorrelated south and east of the Mississippi Delta in winter. Surface-bottom water correlations are substantially lower on the west coast for salinity than for temperature, particularly north of ~42°N (also see Fig. S41).

The modulation of the SST-BWT relationship by the mixed layer depth and bathymetry is explored further in Fig. 9, which shows the monthly SST-BWT anomaly correlations (top row) as a function of the MLD/bottom depth ratio using box and whisker diagrams. The correlations at all grid points within the four CONUS LMEs are aggregated into 10 bins based on the ratio (%) of the climatological MLD relative to the total column depth. The median value for the SST-BWT correlations ranges between ~0.2 in GOMEX and ~0.5 for the NEUS when the MLD is only 10% of the bottom depth. Although there is a very wide range of values at the individual LME grid points (as indicated by the dashed lines), the correlations increase monotonically as the MLD/bathymetry ratio increases in all four LMEs and approaches 1.0 (for the upper 75% of the grid points within an LME) when the MLD reaches the bottom (100%). Similar to SST-BWT, SSS-BWS correlations increase monotonically as the MLD approaches the bottom, with median values exceeding ~0.8 when the MLD is ≥ 70% of the bottom depth (bottom row of Fig.

9). These results confirm the importance of the MLD in linking the conditions at the surface and the bottom on the CONUS shelf.

The decorrelation time scales for SSTs, BWTs and their difference based on monthly anomalies (Fig. 10, left column) are computed using correlation values at lags of 1 to 12 months following the method described in Delsole (2001) and Buckley et al. (2019). For exponentially decaying values, the method provides an average e-folding time scale, but it can also accommodate oscillatory variability. Typical values for SST anomalies are on the order of 2-3 months in the western Atlantic and 2-5 months in the eastern Pacific. There are a few regions with little persistence (≤1 month, the minimum value), including portions of the Gulf Stream, along the SE coast and over much of the GOMEX. (An analysis based on daily values indicates the decay time scale is < 30 days in these regions and <15 days in portions of the Gulf Stream and near the Mississippi Delta; Amaya et al. 2023b). Regions with greater SST persistence, with decorrelation times > 4 months, include portions of GOMA, and west of Baja California and off the Pacific northwest coast, where values can exceed 8 months. Bottom temperature anomaly decay rates generally range from 2-5 months but are much longer (> 10 months) in the central GOMA. SST autocorrelations vary with the seasons, usually with greater persistence in winter than in summer and enhanced winter-to-winter autocorrelations due to the “reemergence mechanism" (Deser et al. 2003; Stock et al. 2015).

In general, the BWT decay rates are longer than those for SST (Fig. 10c); the BWT-SST difference in decay rates is positive at most of the grid points on the shelf in the domain. The BWT decay rates exceed those for SST by one month for most nearshore regions and 2-3 months for mid-shelf areas of the NEUS and GOMEX. The differences are much larger in the northern Gulf of California and GOMA, where they exceed eight months. The greater persistence of GOMA BWT anomalies results from the water in the deep basins being below the pycnocline, and thus isolated from high-frequency surface forcing, and from slower dynamic ocean processes in the Atlantic that influence the water properties that enter the gulf through the Northeast Channel (Du et al., 2021).

The decorrelation times for SSS anomalies are on the order of 2-5 months off the east coast (Fig. 10d), slightly longer than those for SSTs in most locations. The persistence is low (< 2 months) in the GOMEX, but is higher in the Caribbean, especially south of Cuba. The decay time of SSS anomalies varies widely in the Pacific, with rapid decay off the Pacific northwest coast, likely associated with fluctuations in Columbia River outflow, with much longer-lived anomalies farther offshore, as occurs for SST. Patches with higher SSS persistence occur west of Baja California. BWS decay time scales range from one to six months along the east coast (Fig. 10e). While BWS anomalies persist slightly longer than SSS anomalies in the central GOMA, they are less persistent than the BWT anomalies. BWS decay times are generally less than five months around the rest of CONUS but greater than seven months in the northeast corner of the WFS, with even greater persistence in the northern Gulf of California. The BWS-SSS differences (Fig. 10f) exhibit a similar pattern to those of BWT-SST, although the difference is larger for temperature than salinity in the GOMA and vice versa in the western GOMEX and Gulf of California.

The temperature, salinity and mixed layer depth variability as measured by the standard deviation (σ) is computed using monthly anomalies within a season. The SST σ ranges from 0.5 to 1.5 ℃ over most of the CONUS shelf during winter (Fig. 11a). Regions on the CONUS shelf with somewhat greater variability include sections of the eastern seaboard, the WFS, northwestern GOMEX and west of southern Baja California; SST variability is enhanced in the latter region (28°-32°N) primarily during fall (see Fig. 3a). Much higher variability associated with the Gulf Stream occurs on the shelf near Cape Hatteras and east of the shelf off the NEUS coast, likely due to meridional excursions of the current, as well as meandering and mesoscale eddy activity. The pattern of the BWT σ on the shelf (Fig. 11b) is similar to that at the surface during winter. Some regions exhibit stronger BWT than SST variability, including portions of the NEUS shelf, the Gulf of California and on the southwest side of Baja Peninsula (also see Figs. 3a&b), but the bottom temperature variability is slightly lower than at the surface along much of the US west coast. The MLD σ in JFM (Fig. 11c) is less than 20 m over nearly all of the CONUS shelf and less than 5 m over much of the east coast and GOMEX. It is larger beyond the outer edge of the NEUS shelf, where it approaches 50 m.

The SST variability in summer (Fig. 11d) is less than in winter over nearly all of the western Atlantic and GOMEX, except near the center of GOMA. On the west coast, however, the SST variability is slightly larger in summer than in winter (also see Fig. 3a and Fig. S44). The summer BWT variability is stronger than both its winter counterpart and summer SST variability over much of the NEUS shelf and at mid shelf along the entire length of the WFS. The reverse occurs along the US west coast where the BWT variability in JAS is low (σ < 0.5°C). MLD exhibits little variability over the entire CONUS shelf in summer (Fig. 11e).

The surface and bottom water salinity σ in winter and summer are shown in Fig. 12. The SSS variability off the NEUS coast is enhanced in GOMA, along the coast of the mid-Atlantic states and just east of the shelf break in winter. The SSS variability is enhanced in the northern GOMEX with a strong peak near the Mississippi River delta; it is also enhanced in the coastal zone of the Pacific northwest. The area covered by higher SSS variability is more widespread in summer than winter in both regions (Figs. 3 and 12). Salinity variability in these regions is likely driven by fluctuations in outflow from the Mississippi and Columbia rivers, respectively. The BWS σ in both JFM and JAS is similar to the JFM SSS variability, although the variability is highest at the surface in winter in GOMA.

To explore the full range of temperature variability, we present the probability distributions of monthly SST and BWT anomalies for JFM and JAS at all grid squares within the NEUS, SEUS, GOMEX and CCS LMEs in Fig. 13. The amplitudes of the SST and BWT anomalies reach 4.0-5.0°C, except for SSTs in summer in the SEUS and GOMEX, where the anomalies are generally less than $\left| 2.0 \right|$ °C. Also shown in Fig. 13 are higher order metrics: the skewness ($\sum_i^N (X_i - \bar{X})^3 / ((N-1) \times \sigma^3)$) and kurtosis ($\sum_i^N (X_i - \bar{X})^4 / ((N-1) \times \sigma^4)$ - 3), where N is the number of grid points, X_i the individual grid point value and $\bar{X}$ the mean of the distribution; by subtracting 3 the normal distribution has kurtosis = 0. Skewness indicates if the distribution is asymmetrical. Kurtosis provides information about the tails of a distribution: whether it's light (< 0) or heavy tailed with more outliers (> 0), respectively, relative to a Gaussian distribution. The temperatures in the NEUS LME have little skew and are slightly light-tailed during winter and summer, indicating more low amplitude anomalies relative to a Gaussian distribution. The temperatures in the SEUS exhibit a negative skew and positive kurtosis in both seasons. In the

GOMEX, the SST and BWT distributions have heavy tails (leptokurtic distributions), and a slight negative skew. Both the SST and BWT anomalies are positively skewed in the CCS, resulting in more extreme positive temperature anomalies relative to a Gaussian distribution. The CCS is the only LME where ENSO has a strong influence on the SST and BWT distribution: with more positive extremes when La Niña events are excluded (SST and BWT skewness of 0.65 and 2.02, respectively) compared to when El Niño events are excluded (SST and BWT skewness of 0.33 and 0.44). The CCS SST kurtosis values are near zero in winter and one in summer. In contrast, CCS BWTs exhibit exceptionally high kurtosis values (9.3 in JFM and 7.7 in JAS), since BWT anomalies are generally close to zero but occasionally have large amplitudes at some locations and/or times. The results demonstrate that the SST and BWT probability distributions can be significantly different within the same region. Similar plots for SSS and BWS indicate that salinity exhibits a slightly negative skew but very large kurtosis for the four LMEs in both seasons (not shown).

Given the unusual nature of the temperature distribution and the narrowness of the shelf in the CCS, we show the skewness and kurtosis as a function of depth (for all vertical levels) and latitude along the US west coast in Fig. 14. Results are presented as the median value of these two quantities at each latitude in the reanalysis (to account for the variable number of points on the shelf at different latitudes) during JFM and JAS. The distribution measures are very different in winter and summer. During winter large positive values occur for skewness at depths of approximately 80-180 m and between 60-200 m for kurtosis, where the maxima for both occur below the MLD and at greater depths as the latitude increases. Kurtosis values are negative at shallower depths. The temperatures are positively skewed at most latitudes and depths in summer with larger skew within ~40m of the surface poleward of ~35°N and between 40-100 m from 32°-34°N. The kurtosis is also positive with larger magnitudes in these areas but becomes negative at greater depths over most latitudes.

Longer term changes in temperature, as indicated by the linear temperature trend over 1993-2018 for SST and BWT in winter and summer are shown in Fig. 15. The SST trend is positive over most of the domain especially in summer. The trend is statistically significant (95% level based on a Mann-Kendall test) over most of the Atlantic in both winter and summer and in the Gulf of

Mexico and nearf Baja California in summer. The most intense warming, which exceeds 3°C dec^{-1} occurs off the NEUS coast. The intense warming at the surface and at the bottom is consistent with the observational analyses of Pershing et al. (2015) and Kavanugh et al. (2017), respectively. The positive SST trend is most intense east of the shelf break in winter and over central GOMA. The increase in the NEUS SSTs is likely due to a northward shift of the Gulf Stream (Wu et al., 2012; Seidov et al., 2021) as well as warming over the adjacent continent (Hayhoe et al., 2018) and the subsequent eastward advection of the warm air over the ocean. The NEUS warming is consistent with results from models forced with an increase in greenhouse gasses (e.g., Alexander et al., 2018, 2020), although internal climate variability including fluctuations in the Atlantic Meridional Overturning Circulation, contribute to multi-decadal variability (Deser and Phillips, 2021). In addition, the climate change signal is likely to be nonlinear in some regions (Frankignoul et al., 2017, Xu et al., 2022), although a linear estimate appears to be reasonable over ≤ 30-year periods (Alexander et al., 2018; Wang et al., 2022).

The SST exhibits a strong negative trend in a narrow strip along the SEUS coast, with weaker cooling along portions of the northern and western GOMEX coasts during winter. However, the cooling trend all but disappears in summer. The SST trends are generally weaker and of mixed sign in the Pacific in winter, but become more positive in summer. While in many locations on the CONUS shelf the BWT trend reflects that at the surface, there are regions where they are quite different. For example, the bottom temperature in JAS has a negative trend on parts of the southeastern side of the GOMA including Georges Bank, and in the middle of the WFS where the surface exhibits a moderate to strong positive trend. A strong positive BWT trend also occurs at the shelf break along near all of the east and GOMEX coasts and in the northern Gulf of California. The modest BWT cooling along most of the west coast in JFM is replaced by weak warming in JAS. The warming BWT trend is significant in the GOMA and portions of the GOMEX and the north Gulf of California in winter, with more locations exhibiting a significant warming trend along both coasts and in the GOMEX during summer. Only a few points have statistically significant negative trends in either season.

The salinity trends (Fig. 16) indicate that the SSS in the NEUS region is becoming more saline in winter. The trend is reduced in summer over most of the region, although it remains strong in the

608 southwest corner of the LME (mid-Atlantic coast) and there is a small area of freshening in
609 GOMA. SSS exhibits a positive (negative) trend in the eastern (western) GOMEX in winter. The
610 pattern is similar in summer, although there is a relatively strong upward trend in the
611 northeastern part of the gulf located between two areas of freshening. The SSS trends are
612 generally small in the Pacific, although freshening in winter is replaced by salinification in
613 summer along the northwest Pacific coast. The trend in this region is likely associated with
614 changes in Columbia River outflow, which has decreased over the past several decades during
615 summer (Forbes et al., 2019) The bottom water salinity trends generally reflect those at the
616 surface. The positive salinity trends are statistically significant over much of the NEUS in winter,
617 although fewer locations have a significant SSS trend in summer. The SSS and BWS trends are
618 also significant over the southeast Caribbean, western Gulf of Mexico, Gulf of California and
619 roughly one third of the points in the Pacific.
620
621 *Vertical Structure*
622 Finally, we explore conditions through the water column by showing cross sections (locations
623 shown in Fig. 1) of the temperature and salinity climatology and standard deviation for the
624 NEUS, SEUS, GOMEX and the CCS for the four seasons. Fig. 17 displays the transect at
625 42.5°N, which crosses the complex bathymetry of the southern GOMA, extending eastward from
626 the shore including the Wilkinson Basin, Georges Basin, the Northeast Channel and Browns
627 Bank. The mean temperature increases with depth and exhibits a weak thermocline located at
628 approximately 100 m depth across GOMA in JFM. A seasonal thermocline develops at a depth
629 of ~20 m in spring and becomes very intense during summer before weakening in fall. The mean
630 temperatures have a minimum value at ~75 m in spring and summer and relatively warm water (
631 ~10°C) remains throughout the year at ~150 m on the eastern side of Georges Basin (66°W). The
632 greatest variability occurs below the surface layer in the eastern portion of the basin, likely
633 associated with fluctuations of warm Atlantic water on Brown's Banks and entering GOMA
634 through the Northeast Channel.
635
636 The climatological near-surface salinity is relatively fresh in the eastern and western portions of
637 the 42.5°N transect with a maximum that shifts slightly eastward from JFM to OND (Fig. 17
638 bottom). The salinity gradient is strong: west of ~70°W above 50m, at all depths in the eastern

639 portion of the basin, below about 70 m in all seasons, and over the entire water column in
640 summer. Given the temperature profile, salinity maintains the static stability of GOMA,
641 especially below ~70 m and in the northeast channel. Salinity variability is largest in the eastern
642 part of the transect, particularly at depth in spring and near the surface in fall. Enhanced
643 variability also occurs in the upper 50 m across much of GOMA in JFM and between 68°-70°W
644 in AMJ.
645
646 The SEUS cross section (Fig. 18) extends eastward along 32°N (starting near Savannah, GA)
647 into the Atlantic. The maximum mean temperature, associated with the Gulf Stream, occurs in
648 the vicinity of 78°W from the surface to 100 m depth. The climatological temperature gradient is
649 strong on either side of the Gulf Stream below about 50 m, especially on its eastern flank to the
650 shelf break. There is also a strong positive offshore gradient from the coast that extends from the
651 surface to the bottom for depths shallower than ~50 m in fall and winter. The temperature
652 variability is strongest adjacent to the shelf, especially between 50-150 m in JFM and OND. The
653 variability is also somewhat higher in the thermocline to the east of the Gulf Stream. The salinity
654 field is fairly uniform offshore, with strong gradients along the shelf especially in the shallow
655 near-shore region and below ~100 m. The salinity variability is very strong on the shelf at depths
656 of less than ~30 m and along the shelf break but with lower amplitude. The strong climatological
657 gradient and variability in the near shore region is likely associated with freshwater input from
658 rivers entering into the LME (Blanton, 1981), while the strong temperature and salinity gradient
659 along the shelf break may be influenced by the local bathymetric features, including the
660 “Charleston Bump”, and the proximity of the Gulf Stream. The variability is also higher to the
661 east of the Gulf Stream above ~75 m in AMJ and JAS.
662
663 The GOMEX cross section (Fig. 19) extends along 26°N from south Florida to the central Gulf
664 of Mexico. In contrast to the previous cross sections, the climatological temperature and
665 variability vary smoothly. The mean temperatures are colder on the WFS in winter and increase
666 offshore to 85°W, where the temperatures are higher throughout the water column than at other
667 longitudes at the same depth. This depression in the isotherms decreases from spring to summer
668 and is slightly inverted in fall. The vertical temperature gradient is strong and fairly regular over
669 most of the water column below about 100 m in JFM, 30 m in AMJ and JAS and 50 m in OND.

The largest temperature variability occurs offshore at ~89°W at depths of 125-250 m in JFM. As the seasons progress, the maximum σ shifts closer to shore and is quite extensive in OND where it reaches ~3°C between 100-300m at ~87°W. The strong variability is likely associated with fluctuations in the Loop Current, in contrast, there is little variability on the shelf. The vertical temperature gradient remains strong but the variability decreases when the GOMEX transect is located further north (not shown).

The mean salinity profile is fairly uniform across the GOMEX transect, with a slight maximum around 150m that is located in the vicinity of 86°W in winter and spring but closer to the continental slope in fall (Fig. 19). One center of salinity variability is located above 30 m and is confined close to the shelf except in JAS, when it extends over the full transect. A second region of enhanced variability occurs in all seasons below 150 m west of ~86°W.

The west coast transect (Fig. 20) extends offshore from northern California along 40°N. The upper thermocline is fairly diffuse in JFM and slopes upward from ~100 m at 130°W to towards the surface at the coast. It strengthens through spring into summer and nearly reaches the surface as upwelling of fairly uniform cold water acts to compress the isotherms. The greatest temperature variability occurs offshore within the thermocline, with the maximum occurring in fall.

The climatological halocline west of California extends between 50 and 200 m over most of the transect and like temperature, it is compressed and slopes more strongly towards the surface near the coast (Fig. 20). The salinity σ is greatest near the surface and the shore in AMJ, with elevated variability in the same area in JFM and located near the surface but further offshore in JAS. These regions of higher variability appear to be associated with fluctuations in the outflow from the Columbia River (see Figs. 12, S46, S47) and the California Current, which transports water southward along the west coast. Areas of higher variability also occur within the halocline.

Discussion and Conclusions

While coastal ocean conditions have been studied using satellite and *in situ* observations as well as regional ocean models, recently developed fine-scale global ocean reanalyses enable a broader, observationally constrained, three-dimensional view of conditions on continental shelves. Here, we used the 1/12° (~9 km) Global Ocean Reanalysis and Simulations (GLORYS) to examine temperature and salinity (with a focus on surface and bottom waters) and mixed layer depth on the shelf (depth < 400 m) around the continental United States. We examined the climatological seasonal cycle, standard deviation and broader measures of variability, including the persistence, trend, skewness, kurtosis and probability distributions over the period 1993-2019.

A key aspect we examined was the relationship between surface and bottom water conditions on the highly variable US continental shelf and its modulation by the mixed layer depth relative to bathymetric features. In general, the SST and BWT are more tightly coupled at shallower depths during winter when the mixed layer is deep and turbulence can mix the surface and near-bottom waters, as suggested by Schaeffer and Roughan (2017) using *in situ* observations at two locations along the east coast of Australia and by Amaya et al. (2023b) who used the GLORYS reanalysis to investigate bottom water heat waves around North America. Our analyses indicated that this is an important factor in linking SST and BWT anomalies over the US continental shelf, where the SST-BWT relationship is influenced by a number of factors including the bathymetry, the MLD seasonal cycle and other dynamical ocean processes. The Gulf of Maine, with shallow banks, deep basins and a connection to the North Atlantic at depth, illustrates the potential complexity in the relationship between surface and bottom conditions. For example, while the maximum SST occurs in August over the entire gulf, the month with the warmest BWT ranges from September on Georges Bank to as late as March and April in the deep basins in the eastern part of GOMA. The SST and BWT are well correlated (> 0.8) in shallower regions but weakly correlated (< 0.5) in the deeper portions of GOMA, which are below the mixed layer even in winter. The correlations drop significantly at relatively shallow depths in summer but remain relatively unchanged in deeper layers. Sheltered from higher frequency surface forcing, BWT anomalies last longer than SST anomalies by one to two months in most locations, and up to six months in the inner portion of GOMA.

731 The surface-bottom salinity anomaly correlation pattern is similar to that for temperature over
732 most of the continental US shelf, but the GOMA SSS and BWS are nearly uncorrelated during
733 summer. In addition to local mixing, inflow of warmer/saltier water from the Atlantic into the
734 GOMA at depth can result in the decoupling between conditions at the surface and bottom. Other
735 processes that can separate conditions on the bottom from the surface include freshwater outflow
736 from rivers, especially the Mississippi and Columbia, upwelling, especially along the west coast
737 in summer, interactions with currents, such as the Loop Current on the West Florida Shelf (He
738 and Weisberg 2003), and vertical displacement of the pycnocline where it intersects the shelf, as
739 is often the case along the US west coast. The SSS decorrelation time ranges from about 1 to 10
740 months over the full domain and is slightly longer than those for SSTs over most of the western
741 Atlantic. SSS anomalies decay rapidly in the northern GOMEX and off the Pacific northwest
742 coast, likely associated with variability in the discharge from the Mississippi and Columbia
743 rivers, respectively. The BWS-SSS values are generally similar to those of BWT-SST.
744
745 The monthly SST σ ranges from 0.5 to 1.5 ℃ over most of the CONUS shelf during winter, with
746 somewhat greater variability in parts of the east coast, the WFS, northwestern GOMEX and west
747 of southern Baja California. The BWT and SST variability patterns are similar during winter,
748 when some regions exhibit stronger BWT than SST variability, including portions of the NEUS
749 shelf, and on either side of Baja Peninsula. The BWT variability in summer is stronger than both
750 its winter counterpart and summer SST variability over much of the NEUS shelf and at mid shelf
751 along the entire length of the WFS.
752
753 The SST anomalies in SEUS and GOMEX, and especially the BWT in the CCS LME, exhibit
754 strong kurtosis, indicating more low amplitude anomalies relative to a Gaussian distribution. In
755 addition, the kurtosis over the depth of the water column in the CCS changes between winter and
756 summer, where it is negative at depths shallower than ~80 m and positive between
757 approximately 80-200 m in winter and nearly the reverse in summer. Both the SST and BWT
758 CCS anomalies are positively skewed due to more extreme positive temperature anomalies than
759 negative in the CCS. The processes responsible for the large departures from a normal
760 distribution require further study, as they have strong influence on extreme temperatures
761 including marine heat waves.

We have conducted a broad survey of ocean conditions around the margins of the continental United States with a goal of encouraging more detailed analyses using high-resolution ocean reanalyses, such as GLORYS. While studies evaluating recent ocean reanalyses are being conducted, better understanding of how well they represent conditions and processes should lead to improvements in the data, models and assimilation systems used to create them. These advances may be especially critical in coastal regions, as most global reanalysis systems have been designed for the open ocean.

Acknowledgements

We thank the NOAA Climate Program Office, including the Modeling, Analysis, Predictions and Projections (MAPP) Program for funding this project. CD and AP received support through grant NOAA #NA20OAR4310378.

Data Availability

All of the GLORYS version 12 output provided by the Copernicus Marine Environmental Monitoring Service (CMEMS) is available at: https://resources.marine.copernicus.eu/products.

References

Alexander M.A., Scott, J.D., Friedland, K.D., Mills, K.E., Nye, J.A., Pershing, A.J., and Thomas, A. C., 2018. Projected sea surface temperatures over the 21st century: Changes in the mean, variability and extremes for large marine ecosystem regions of Northern Oceans. Elementa: Science of the Anthropocene, 6(1):9, DOI: http://doi.org/10.1525/elementa.191

Alexander, M.A., Shin, S., Scott, J.D., Curchitser, E., and Stock, C., 2020: The Response of the Northwest Atlantic Ocean to Climate Change J. Clim., 33(2): 405–428. DOI: https://doi.org/10.1175/JCLI-D-19-0117.1.

Amaya D.J., Alexander, M.A., Jacox, M.G., and Scott, J.D., 2023a. An evaluation of high-resolution ocean reanalyses in the California Current System. Prog. Oceanogr., 210, 102951. https://doi.org/10.1016/j.pocean.2022.102951.

Amaya D.J., Alexander, M.A., Jacox, M.G., Scott, J.D., Deser, C. Capotondi, A., and Phillips, A. 2023b. Bottom marine heatwaves along the continental shelves of North America. Nat. Commun. 14, 1038. https://doi.org/10.1038/s41467-023-36567-0

Amaya, D.J., Jacox, M.G., Dias, J., Alexander, M.A., Karnauskas, K.B., Scott, J.D., and Gehne, M., 2022. Subseasonal-to-seasonal forecast skill in the California Current System and its connection to coastal Kelvin waves. J. Geophys. Res.: Oceans, 127(1), e2021JC017892. https://doi. org/10.1029/2021JC017892

Barber B.J., and Blake N.J., 2006. Reproductive physiology. In: Shumway SE, Parsons GJ, editors. Scallops: Biology, Ecology, and Aquaculture: Elsevier. pp. 357–416.

Becker, E.A., Forney, K.A., Fiedler, P.C., Barlow, J., Chivers, S.J., Edwards, C.A., Moore, A.M. and Redfern, J.V., 2016. Moving towards dynamic ocean management: How well do modeled ocean products predict species distributions? Remote Sens., 8(2), 149. https://doi.org/10.3390/rs8020149

Blanton, J.O., 1981. Ocean Currents along a Nearshore Frontal Zone on the Continental Shelf of the Southeastern United States, J. Phys. Oceanogr., 11(12), 1627-1637. Retrieved https://doi.org/10.1175/1520-0485(1981)011<1627:OCAANF>2.0.CO;2

Blanton B.O., Aretxabaleta, A., Werner, F.E., and Seim, H.E., 2003. Monthly climatology of the continental shelf waters of the South Atlantic Bight. J. Geophys. Res. - Oceans, 108(C8). https://doi.org/10.1029/2002JC001609

Block, B.A., Jonsen, I.D., Jorgensen, S.J., Winship, A.J., Shaffer, S.A., Bograd, S.J., et al. 2011 Tracking apex marine predator movements in a dynamic ocean. *Nature* 475(7354): 86–90. DOI: https:// doi.org/10.1038/nature10082

Bograd, S.J., Checkley, D.A., Wooster, W.S., 2003. CalCOFI: a half century of physical, chemical, and biological research in the California Current System, Deep Sea Res. Part II: Topical Studies in Oceanography, 50, (14–16), 2349-2353, ISSN 0967-0645 https://doi.org/10.1016/S0967-0645(03)00122-X.

Brown, W.S., and Beardsley, R.C., 1978. Winter Circulation in the Western Gulf of Maine: Part 1. Cooling and Water Mass Formation, J. Phys. Oceanogr., 8(2), 265-277. Retrieved Oct 27,

2022, from https://journals.ametsoc.org/view/journals/phoc/8/2/1520-0485_1978_008_0265_wcitwg_2_0_co_2.xml

Buckley, M.W., DelSole, T., Lozier, M.S., and Li, L., 2019. Predictability of North Atlantic Sea Surface Temperature and Upper-Ocean Heat Content, J. Clim., 32(10), 3005-3023. https://journals.ametsoc.org/view/journals/clim/32/10/jcli-d-18-0509.1.xml

Cai, C., Kwon, Y.-O., Chen, Z., and Fratantoni, P., 2021: Mixed layer depth climatology over the Northeast U.S. continental shelf (1993-2018). Cont. Shelf Res., 231, 104611. https://doi.org/10.1016/j.csr.2021.104611.

Cai, W.-J., Hu, X., Huang, W.-J., Jiang, L.-Q., Wang, Y., Peng, T.-H., and Zhang, X., 2010, Alkalinity distribution in the western North Atlantic Ocean margins, J. Geophys. Res.: Oceans, 115(C8), C08014, doi:10.1029/2009JC005482.

Carter, B.R., Bittig, H.C., Fassbender, A.J., Sharp, J.D., Takeshita, Y., Xu, et al., L., 2021. New and updated global empirical seawater property estimation routines. Limnol. Oceanogr. Methods, **19**: 785-809. https://doi.org/10.1002/lom3.10461

Carton, J.A., Chepurin, G., Cao, X., and Giese, B., 2000. A Simple Ocean Data Assimilation Analysis of the Global Upper Ocean 1950–95. Part I: Methodology, J. Phys. Oceanogr., *30*(2), 294-309. doi: https://doi.org/10.1175/1520-0485(2000)030<0294:ASODAA>2.0.CO;2

Castillo-Trujillo, A. C., Kwon, Y.-O., Fratantoni, P., Chen, K., Alexander, M., and Saba V., 2023, An evaluation of eight global ocean reanalyses for the Northeast U.S. continental shelf. Prog. Oceanogr., submitted. https://drive.google.com/drive/u/0/folders/1HGO4jbrpnklvusZO5rtdQqdqEZtDZgDL

Chamberlain, M.A., Oke, P.R., Fiedler, R.A.S., Beggs, H.M., Brassington, G.B., and Divakaran, P., 2021. Next generation of Bluelink ocean reanalysis with multiscale data assimilation: BRAN2020, Earth Syst. Sci. Data, 13, 5663–5688, https://doi.org/10.5194/essd-13-5663-2021.

Chen, Z., Kwon, Y.-O., Chen, K., Fratantoni, P., Gawarkiewicz, G., Joyce, T.M., Miller, T.J., et al., 2021. Seasonal prediction of bottom temperature on the northeast U.S. Continental shelf. J. Geophys. Res.: Oceans. 126(5), https://doi.org/10.1029/2021JC017187.

Cheng, L., Trenberth, K.E., Gruber, N., Abraham, J.P., Fasullo, J.T., Li, G., Mann, M.E., Zhao, X., and Zhu, J., 2020. Improved Estimates of Changes in Upper Ocean Salinity and the

Hydrological Cycle, J. Clim., 33(23), 10357-10381. https://journals.ametsoc.org/view/journals/clim/33/23/jcliD200366.xml

de Boyer Montégut, C., Madec, G., Fischer, A.S., Lazar, A., and Iudicone, D. 2004. Mixed layer depth over the global ocean: An examination of profile data and a profile-based climatology, *J. Geophys. Res.*, 109, C12003, doi:10.1029/2004JC002378.

de Souza, J.M.A.C., Couto, P., Soutelino, R., and Roughan, M., 2021. Evaluation of four global ocean reanalysis products for New Zealand waters–A guide for regional ocean modelling. N. Z. J. Mar. Freshw. Res., 55(1), 132–155. https://doi.org/10.1080/00288330.2020.1713179

Dee, D.P., Uppala, S.M., Simmons, A.J., Berrisford, P., Poli, P., Kobayashi, S., et al., 2011. The ERA-Interim Reanalysis: Configuration and Performance of the Data Assimilation System. Q.J.R. Meteorol. Soc. 137, 553–597. doi:10.1002/qj.828

DelSole, T., 2001. Optimally persistent patterns in time-varying fields. J. Atmos. Sci., 58, 1341–1356, https://doi.org/10.1175/1520-0469(2001)058<1341:OPPITV>2.0.CO;2.

Deser, C., and Phillips, A.S., 2021. Defining the internal component of Atlantic Multidecadal Variability in a changing climate. Geophys. Res. Lett., 48, e2021GL095023, doi: 10.1029/2021GL095023.

Deser, C., Alexander, M.A., and Timlin, M.S., 2003. Understanding the Persistence of Sea Surface Temperature Anomalies in Midlatitudes, J. Clim., 16(1), 57-72. https://journals.ametsoc.org/view/journals/clim/16/1/1520-0442_2003_016_0057_utposs_2.0.co_2.xml

Deutsch, C., Ferrel, A., Seibel, B., Pörtner, H.O. and Huey, R.B., 2015. Climate change tightens a metabolic constraint on marine habitats. Science 348: 1132–1135. DOI: https://doi.org/10.1126/science.aaa1605

Drinkwater, KF, Beaugrand, G, Kaeriyama, M, Kim,S, Ottersen, G, Perry, R, et al. 2010. On the processes linking climate to ecosystem changes. J. Mar. Sys. 79: 374–388. DOI: https://doi.org/10.1016/j. jmarsys.2008.12.014

Du, J., Zhang, W.G., and Li, Y., 2021. Variability of deep water in Jordan Basin of the Gulf of Maine: influence of Gulf Stream warm core rings and the Nova Scotia current. J. Geophys. Res.: Oceans, 126(5), https://doi.org/10.1029/2020JC017136

Edwards, M. and Richarson, A.J., 2004. Impact of climate change on marine pelagic phenology and trophic mismatch. Nature **430**: 881–884. DOI: https://doi. org/10.1038/nature02808

Erichsen, A.C., and Middelboe, A.L., 2022. Introduction to the special series, The future of marine environmental monitoring and assessment. Integr. Environ. Assess. Manag. 18(4), 888-891. https://doi.org/10.1002/ieam.4640

Forbes, W.L., Mao, J., Ricciuto, D.M., Kao, S.-C., Shi, X., Tavakoly, A.A., et al., 2019. Streamflow in the Columbia River Basin: Quantifying changes over the period 1951-2008 and determining the drivers of those changes. Water Resour. Res., 55, 6640–6652. https://doi.org/10.1029/2018WR024256

Fox-Kemper, B., Johnson, L., and Qiao, F. 2022. Ocean Mixing, Chapter 4 - Ocean Near-Surface Layers. Editor(s): Meredith, M., Garabato, A.N. in Ocean Mixing, Elsevier, Pages 65-94, ISBN 9780128215128, https://doi.org/10.1016/B978-0-12-821512-8.00011-6.

Fox-Kemper, B., and coauthors, 2021. Ocean, Cryosphere and Sea Level Change. In Climate Change 2021: The Physical Science Basis. Contribution of Working Group I to the Sixth Assessment Report of the Intergovernmental Panel on Climate Change [Masson-Delmotte, V., P. Zhai, A. Pirani, S.L. Connors, C. Péan, S. Berger, N. Caud, Y. Chen, L. Goldfarb, M.I. Gomis, M. Huang, K. Leitzell, E. Lonnoy, J.B.R. Matthews, T.K. Maycock, T. Waterfield, O. Yelekçi, R. Yu, and B. Zhou (eds.)]. Cambridge University Press, Cambridge, United Kingdom and New York, NY, USA, pp. 1211–1362, doi:10.1017/9781009157896.011.

Frankignoul, C., Gastineau, G., and Kwon, Y., 2017. Estimation of the SST Response to Anthropogenic and External Forcing and Its Impact on the Atlantic Multidecadal Oscillation and the Pacific Decadal Oscillation, J. Clim., 30(24), 9871-9895. https://journals.ametsoc.org/view/journals/clim/30/24/jcli-d-17-0009.1.xml

Fry, F.E.J., 1971. The effect of environmental factors on the physiology of fish. In: Hoar, WS and Randall, DJ (eds.), Fish physiol., 1–98. Academic Press, New York. DOI: https://doi.org/10.1016/ S1546-5098(08)60146-6

Haltuch, M.A., Tolimieri, N., Lee, Q. and Jacox, M.G., 2020. Oceanographic drivers of petrale sole recruitment in the California Current Ecosystem. Fish. Oceanogr., 29(2), 122-136. https://doi.org/10.1111/fog.12459

Harvey, C.J., 2009. Effects of temperature change on demersal fishes in the California Current: a bioenergetics approach. Can. J. Fish. Aquat. Sci. 66(9): 1449-1461. https://doi.org/10.1139/F09-087

Hayhoe, K., Wuebbles, D.J., Easterling, D.R., Fahey, D.W., Doherty, S., Kossin, J., et al., 2018: Our Changing Climate. In Impacts, Risks, and Adaptation in the United States: Fourth National Climate Assessment, Volume II [Reidmiller, D.R., C.W. Avery, D.R. Easterling, K.E. Kunkel, K.L.M. Lewis, T.K. Maycock, and B.C. Stewart (eds.)]. U.S. Global Change Research Program, Washington, DC, USA, pp. 72–144. doi: 10.7930/NCA4.2018.CH2

He, Q., and Silliman, B.R., 2019. Climate Change, Human Impacts, and Coastal Ecosystems in the Anthropocene, Curr. Biol., 29(19), R1021-R1035, ISSN 0960-9822, https://doi.org/10.1016/j.cub.2019.08.042.

He, R., and Weisberg, R.H., 2003. A Loop Current Intrusion Case Study on the West Florida Shelf, J. Phys. Oceanogr., 33(2), 465-477 https://journals.ametsoc.org/view/journals/phoc/33/2/1520-0485_2003_033_0465_alcics_2.0.co_2.xml.

Hedger, R., Mckenzie, E., Heath, M., Wright, P., Scott, B.E., Gallego-Fernandez, J., and Andrews, J., 2004. Analysis of the spatial distributions of mature cod (Gadus morhua) and haddock (Melanogrammus aeglefinus) abundance in the North Sea (1980-1999) using generalised additive models. Fish. Res., 70, 17-25. https://doi.org/10.1016/j.fishres.2004.07.002

Helaire, L.T., Talke, S.A., Jay, D.A., & Mahedy, D., 2019. Historical changes in Lower Columbia River and estuary floods: A numerical study. J. of Geophys. Res.: Oceans, 124, 7926– 7946. https://doi.org/10.1029/2019JC015055

Hunt, G.L., Coyle, K.O., Eisner, L.B., Farley, E.V., Heintz, R.A., Mueter, F., et al. 2011. Climate impacts on eastern Bering Sea foodwebs: a synthesis of new data and an assessment of the Oscillating Control Hypothesis. ICES J. Mar. Sci. **68**: 1230–1243. DOI: https://doi.org/10.1093/icesjms/fsr036

Huyer, A., 1983. Coastal upwelling in the California current system, Prog. Oceanogr., 12(3), Pages 259-284, ISSN 0079-6611, https://doi.org/10.1016/0079-6611(83)90010-1.

Jacox, M.G., Moore, A.M., Edwards, C.A., and Fiechter J., 2014. Spatially resolved upwelling in the California Current System and its connections to climate variability, Geophys. Res. Lett., 41, doi:10.1002/2014GL059589.

Jang, C.J., Park, J., Park, T., and Yoo, S. 2011. Response of the ocean mixed layer depth to global warming and its impact on primary production: a case for the North Pacific Ocean. ICES J. Mar. Sci., 68(6), 996–1007. https://doi.org/10.1093/icesjms/fsr064

Kalnay, E., Kanamitsu, M., Kistler, R., Collins, W., Deaven, D., Gandin, L., et al., 1996. The NCEP/NCAR 40-Year Reanalysis Project, Bull. Amer. Met. Soc., *77*(3), 437-472. doi: https://doi.org/10.1175/1520-0477(1996)077<0437:TNYRP>2.0.CO;2

Kavanaugh, M.T., Rheuban, J.E., Luis, K.M.A., and Doney, S.C. 2017. Thirty-three years of ocean benthic warming along the U.S. Northeast Continental Shelf and Slope: Patterns, drivers, and ecological consequences. J. Geophys. Res.: Oceans, 122, 9399–9414. https://doi.org/10.1002/2017JC012953

Kristiansen, T., Drinkwater, K.F., Lough, R.G. and Sundby, S., 2011. Recruitment variability in North Atlantic cod and match-mismatch dynamics. Plos One 6. DOI: https://doi.org/10.1371/journal. pone.0017456

Legaard, K.R., and Thomas, A.C., 2006. Spatial patterns in seasonal and interannual variability of chlorophyll and sea surface temperature in the California current. J. Geophys. Res.: Oceans, 111(C6), 1–21. https://doi.org/10.1029/2005JC003282

Lellouche, J.M., Eric, L., Romain, L.G., Gilles, B.B., Angélique, M., Marie, D., et al., 2021. The Copernicus Global 1/12° Oceanic and Sea Ice GLORYS12 Reanalysis. Front. Earth Sci., 9. https://doi.org/10.3389/feart.2021.698876

Li, Y., Fratantoni, P.S., Chen, C., Hare, J.A., Sun, Y., Beardsley, R.C., and Ji, R., 2015. Spatiotemporal patterns of stratification on the Northwestern Atlantic shelf. Prog. Oceanogr. 134, 123–137. ISSN 0079-6611, https://doi.org/10.1016/j.pocean.2015.01.003

Liu, M., and Tanhua, T. 2021. Characteristics of Water Masses in the Atlantic Ocean. Ocean Sci., 17, 463–486, https://doi.org/10.5194/os-17-463-2021

Madec, G., the NEMO team, 2008. NEMO ocean engine. Note du Pôle de modelisation, Institut Pierre-Simon Laplace (IPSL), France, No. 27. ISSN, 1288-1619.

Miller, A.S., Shepherd, G.R., and Fratantoni, P.S., 2016. Offshore habitat preference of overwintering juvenile and adult black sea bass, *Centropristis striata*, and the relationship to year-class success. PLoS ONE 11(1): e0147627. pmid:26824350

Monterey, G.I., and S. Levitus, 1997: Seasonal Variability of Mixed Layer Depth for the World Ocean. NOAA Atlas NESDIS 14, 5 pp. and 87 figs.

Moore A.M., Martin M.J., Akella, S., Arango H.G., Balmaseda M., Bertino L., et al., 2019. Synthesis of Ocean Observations Using Data Assimilation for Operational, Real-Time and Reanalysis Systems: A More Complete Picture of the State of the Ocean. Front. Mar. Sci. 6:90. doi: 10.3389/fmars.2019.00090

Mountain, D.G., and Manning, J.P., 1994. Seasonal and interannual variability in the properties of the surface waters of the Gulf of Maine. Cont. Shelf Res. 14(13), 1555–1581. https://doi.org/10.1016/0278-4343(94)90090-6

Mueter, F.J., Broms, C., Drinkwater, K.F., Friedland, K.D., Hare, J.A., Hunt, G.L., et al., 2009. Ecosystem responses to recent oceanographic variability in high-latitude Northern Hemisphere ecosystems. Prog. Oceanogr. 81, 93–110. DOI: https://doi.org/10.1016/j. pocean.2009.04.018

National Marine Fisheries Service. 2022. Fisheries Economics of the United States, 2019. U.S. Dept. of Commerce, NOAA Tech. Memo. NMFS-F/SPO-229A, 236 p.

Neveu, E., Moore, A.M., Edwards, C.A., Fiechter, J., Drake, P., Crawford, W. J., and coauthors, 2016. An historical analysis of the California Current circulation using ROMS 4D-Var: System configuration and diagnostics. Ocean Model., 99, 133–151. https://doi.org/10.1016/j.ocemod.2015.11.012

Nye, J.A., Link, J.S., Hare, J.A. and Overholtz, W.J., 2009. Changing spatial distribution of fish stocks in relation to climate and population size on the Northeast United States continental shelf. Mar Ecol. Prog. Ser. 393: 111–129. DOI: https://doi.org/10.3354/ meps08220

Ottersen, G., Kim, S., Huse, G., Polovina, J.J. and Stenseth, N.C., 2010 Major pathways by which climate may force marine fish populations. J. Mar. Sys. **79**: 343–360. DOI: https://doi.org/10.1016/ j.jmarsys.2008.12.013

Pershing, A.J., Alexander, M.A., Hernandez, C.M., Kerr, L.A., Le Bris, L., Mills, K.E., et al., 2015. Slow adaptation in the face of rapid warming leads to the collapse of Atlantic cod in the Gulf of Maine. Science, 13;350(6262):809-12. doi: 10.1126/science.aac9819.

Pinsky, M.L., Worm, B., Fogarty, M.J., Sarmiento, J.L., and Levin, S.A., 2013. Marine taxa track local climate velocities. Science 341(6151), 1239–1242. PMID: 24031017. DOI: https://doi.org/10.1126/ science.1239352

Planque, B. and Fredou, T., 1999. Temperature and the recruitment of Atlantic cod (Gadus morhua). Can. J. Fish Aquat. Sci., 56, 2069–2077. DOI: https://doi. org/10.1139/f99-114

Rivkin, R.B. and Legendre, L., 2001. Biogenic carbon cycling in the upper ocean: effects of microbial respiration. Science, 291(5512): 2398–2400. DOI: https://doi. org/10.1126/science.291.5512.2398

Roemmich, D., Alford, M.H., Claustre, H., Johnson, K., King, B., Moum, J., et al., 2019. On the Future of Argo: A Global, Full-Depth, Multi-Disciplinary Array. Front. Mar. Sci., 6, https://doi.org/10.3389/fmars.2019.00439

Rossby, T., and Gottlieb, E., 1998. The Oleander Project: Monitoring the variability of the Gulf Stream and adjacent waters between New Jersey and Bermuda, Bul. Amer. Met. Soc., 79(1), 5-18. https://journals.ametsoc.org/view/journals/bams/79/1/1520-0477_1998_079_0005_topmtv_2_0_co_2.xml

Rudnick, D. L., 2016. Ocean Research Enabled by Underwater Gliders. Ann. Rev. Mar. Sci. 8(1), 519-541. https://doi.org/10.1146/annurev-marine-122414-033913

Russo, C.S., Veitch, J., Carr, M., Fearon, G., and Whittle, C., 2022. An Intercomparison of Global Reanalysis Products for Southern Africa's Major Oceanographic Features. Front. Mar. Sci., 9:837906, https://www.frontiersin.org/articles/10.3389/fmars.2022.837906

Salisbury, J.E., and Jönsson, B.F., 2018. Rapid warming and salinity changes in the Gulf of Maine alter surface ocean carbonate parameters and hide ocean acidification. Biogeochemistry, 141, 401-418, 10.1007/s10533-018-0505-3

Sardeshmukh, P.D., Compo, G.P., and Penland, C., 2015. Need for caution in interpreting extreme weather statistics, J. Clim., 28(23), 9166-9187. https://journals.ametsoc.org/view/journals/clim/28/23/jcli-d-15-0020.1.xml

Scavia, D., Field, J.C., Boesch, D.F., Buddemeier, R.W., Burkett, V., Cayan, D. R., et al., 2002. Climate change impacts on U.S. Coastal and Marine Ecosystems. Estuaries, 25, 149–164 (2002). https://doi.org/10.1007/BF02691304

Schaeffer, A., and Roughan, M., 2017. Subsurface intensification of marine heatwaves off southeastern Australia: The role of stratification and local winds, Geophys. Res. Lett., 44, 5025– 5033, doi:10.1002/2017GL073714.

Schroeder, I.D., J.A. Santora, A. M. Moore, C. A. Edwards, J. Fiechter, E. L. Hazen, S. J. Bograd, J. C. Field, and B. K. Wells, 2014. Application of a data-assimilative regional ocean modeling system for assessing California Current System ocean conditions, krill, and juvenile rockfish interannual variability, Geophys. Res. Lett., 41, 5942–5950, doi:10.1002/2014GL061045.

Seidov, D., Mishonov, A., and Parsons, R., 2021. Recent warming and decadal variability of Gulf of Maine and Slope Water, Limnol. Oceanogr., 66(9), doi:10.1002/lno.1189

Sherman, K., and Duda, A.M., 1999. Large marine ecosystems: an emerging paradigm for fishery sustainability. Fisheries, 24, 15–26. https://doi.org/10.1577/1548-8446(1999)024<0015: LME>2.0.CO;2.

Stock, C., Pegion, K., Vecchi, G., Alexander, M., Tommasi, D., Bond, N., et al., 2015: Seasonal Sea Surface Temperature Anomaly Prediction for Coastal Ecosystems. Prog. Oceanogr., 137, 219-236. doi:10.1016/j.pocean.2015.06.007

Storto, A., Alvera-Azcárate, A., Balmaseda, M.A., Barth, A., Chevallier, M., Counillon, F., et al., 2019. Ocean reanalyses: Recent advances and unsolved challenges. Front. Mar. Sci., 6, https://doi.org/10.3389/fmars.2019.00418

Sura, P., and Sardeshmukh, P.D., 2008: A global view of non-Gaussian SST variability. J. Phys. Oceanogr., 38, 639–647, doi:10.1175/2007JPO3761.1.

Szekely, T., Gourrion, J., Pouliquen, S., and Reverdin, G., 2019. The CORA 5.2 dataset: global in-situ temperature and salinity measurements dataset. Data description and validation. The CORA 5.2 Dataset: Global in-Situ Temperature and Salinity Measurements Dataset. Data Description and Validation, 1–20. https://doi.org/10.5194/os-2018-144

Tittensor, D.P., Mora, C., Jetz, W., Lotze, H.K., Ricard, D., Berghe, E.V. and Worm, B., 2010. Global patterns and predictors of marine biodiversity across taxa. Nature 466(7310): 1098–1101. DOI: https:// doi.org/10.1038/nature09329

Tolimieri, N., Haltuch, M.A., Lee, Q., Jacox, M.G. and Bograd, S.J., 2018. Oceanographic drivers of sablefish recruitment in the California Current. Fish. Oceanogr., 27(5), 458-474. https://doi.org/10.1111/fog.12266

Tomczak, M., 1999. Some historical, theoretical and applied aspects of quantitative water mass analysis. J. Mar. Res., 57, 275–303.

Wang, S., Jing, Z., Sun, D., Shi, J., and Wu, L., 2022. A new model for isolating the marine heatwave changes under warming scenarios, J. Atmos. Ocean Technol., 39(9), 1353-1366. https://journals.ametsoc.org/view/journals/atot/39/9/JTECH-D-21-0142.1.xml

Wu, L., Cai, W., Zhang, L., Nakamura, H., Timmermann, A., Joyce, T.M., et al., 2012: Enhanced warming over the global subtropical western boundary currents. Nature Climate Change. DOI: 10.1038/NCLIMATE1353.

Xie, J., Zhu, J., and Li, Y., 2008. Assessment and inter-comparison of five high-resolution sea surface temperature products in the shelf and coastal seas around China. Continental Shelf Research, 28(10–11), 1286–1293. https://doi.org/10.1016/j.csr.2008.02.020

Xu, T., Newman, M, Capotondi, A., Stevenson, S., Di Lorenzo, E., and Alexander, M., 2022. An increase in marine heatwaves without significant changes in surface ocean temperature variability. Nat. Commun., 13, 7396, doi: 10.1038/s41467-022-34934-x.

Younes A.F., Cerrato R.M., Nye J.A., 2020. Overwintering survivorship and growth of young-of-the-year black sea bass Centropristis striata. PLoS ONE 15(8): e0236705. https://doi.org/10.1371/journal.pone.0236705

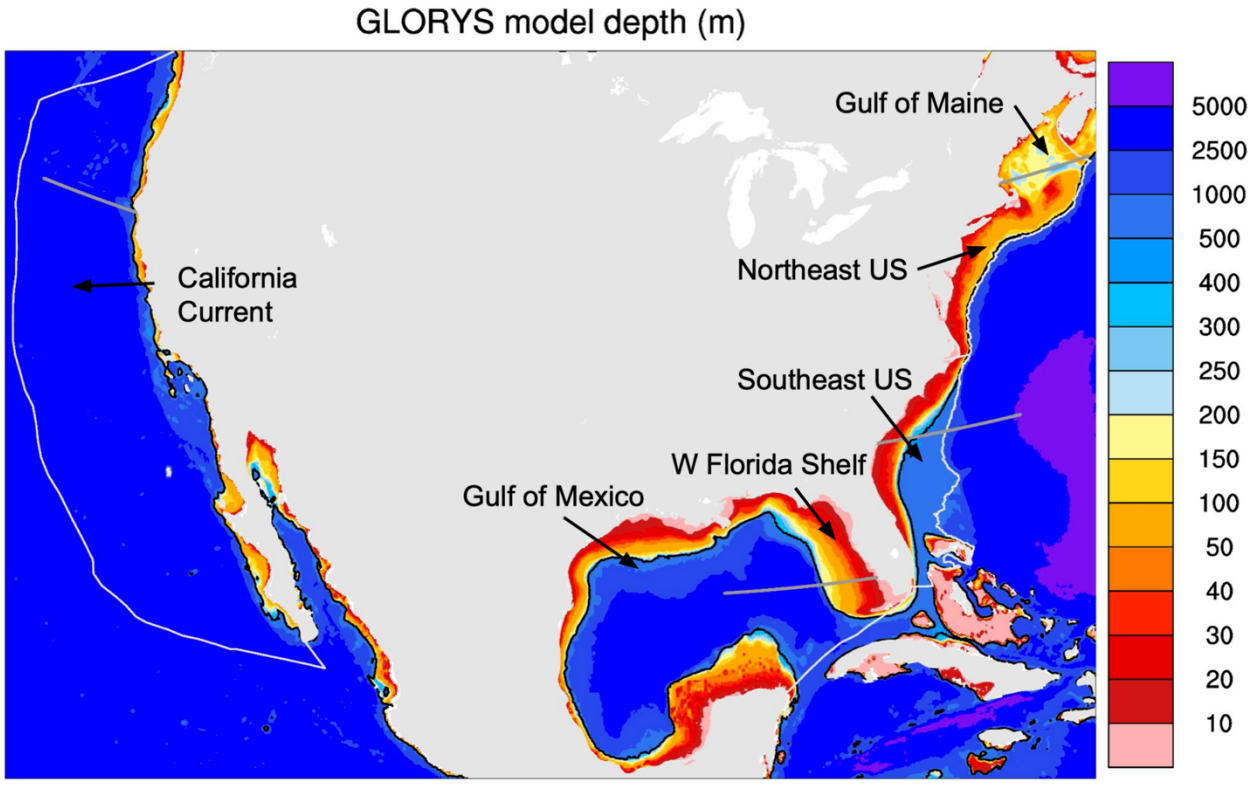

Fig. 1. GLORYS bathymetric depth (m), LME boundaries (light gray line), 400m isobath (black contour line). Cross-section locations for Figs.17-20 (dark gray lines).

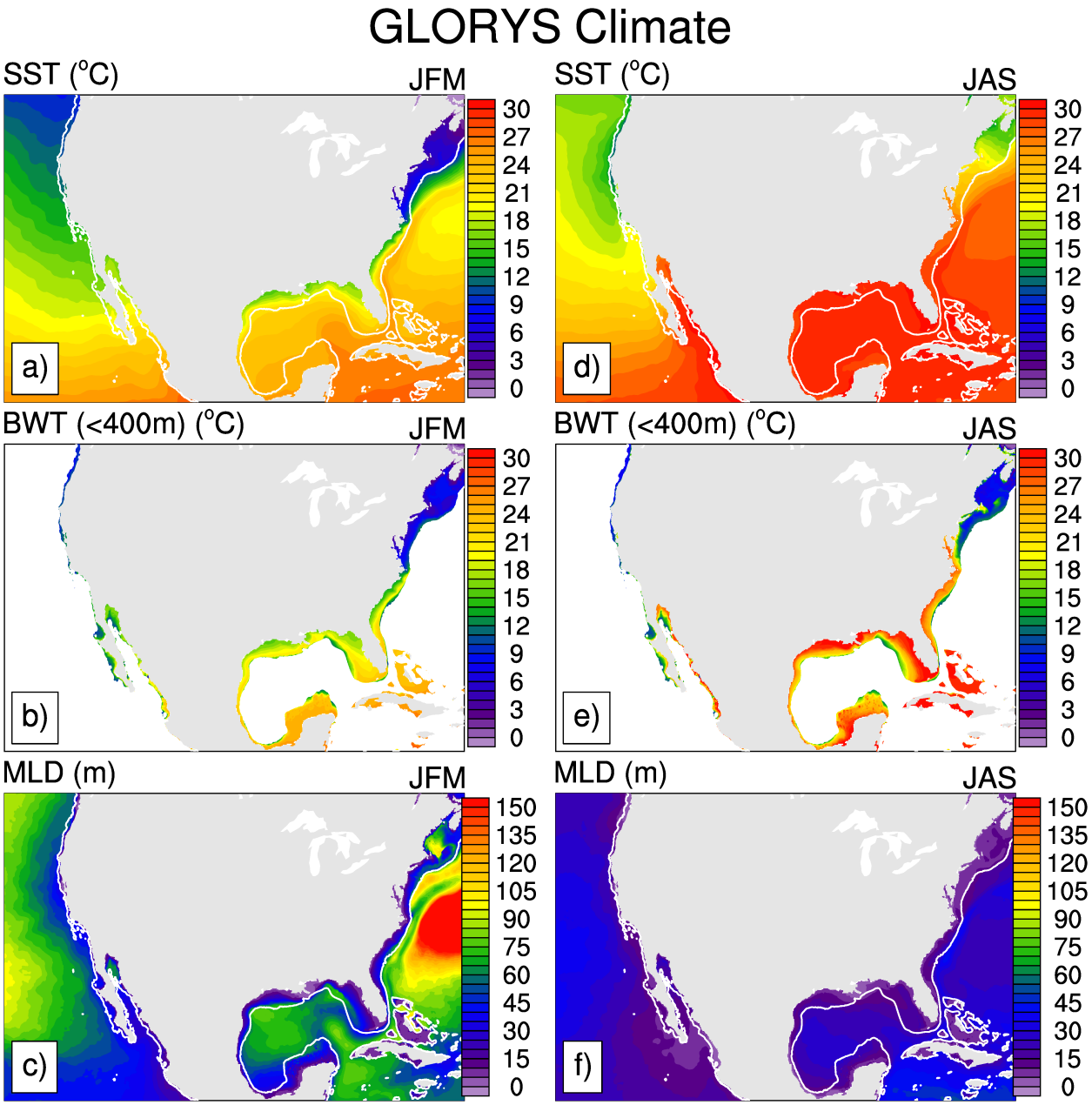

Fig. 2. GLORYS seasonal mean climate (a,d) SST, (b,e) BWT < 400m, (c,f) MLD for JFM (left) and JAS (right). The 400m isobath (gray line) is shown in (a,c,d,f); only bottom water values < 400 m are plotted in all figures.

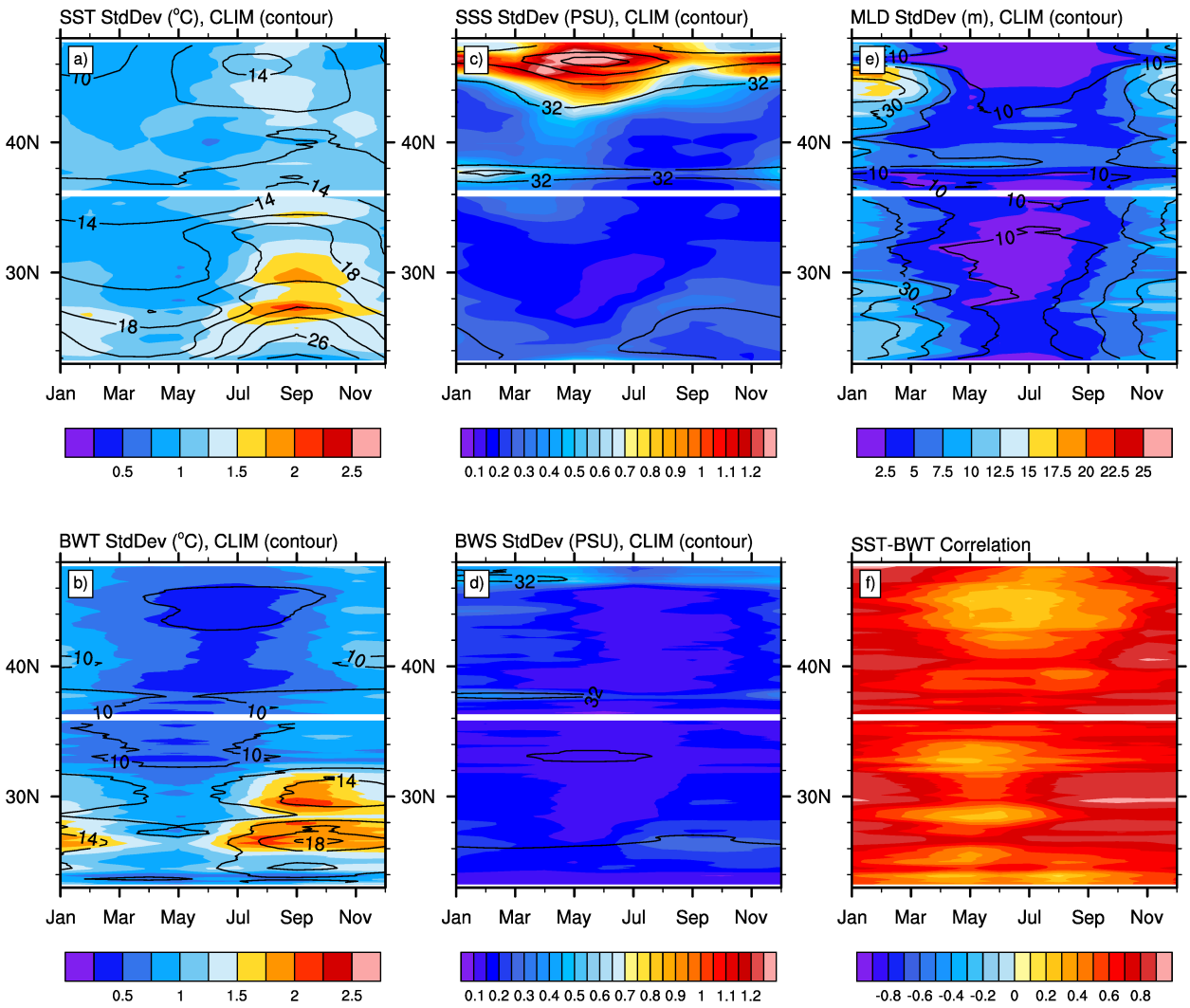

Fig. 3. The seasonal cycle as a function of latitude for coastal (< 400m) points in the CCS based on monthly averaged values for all coastal longitudes of the climatology (contours) and standard deviation (shading) for (a) SST, (b) BWT, (c) SSS, (d) BWS, (e) MLD, and (f) correlation between SST and BWT anomalies.

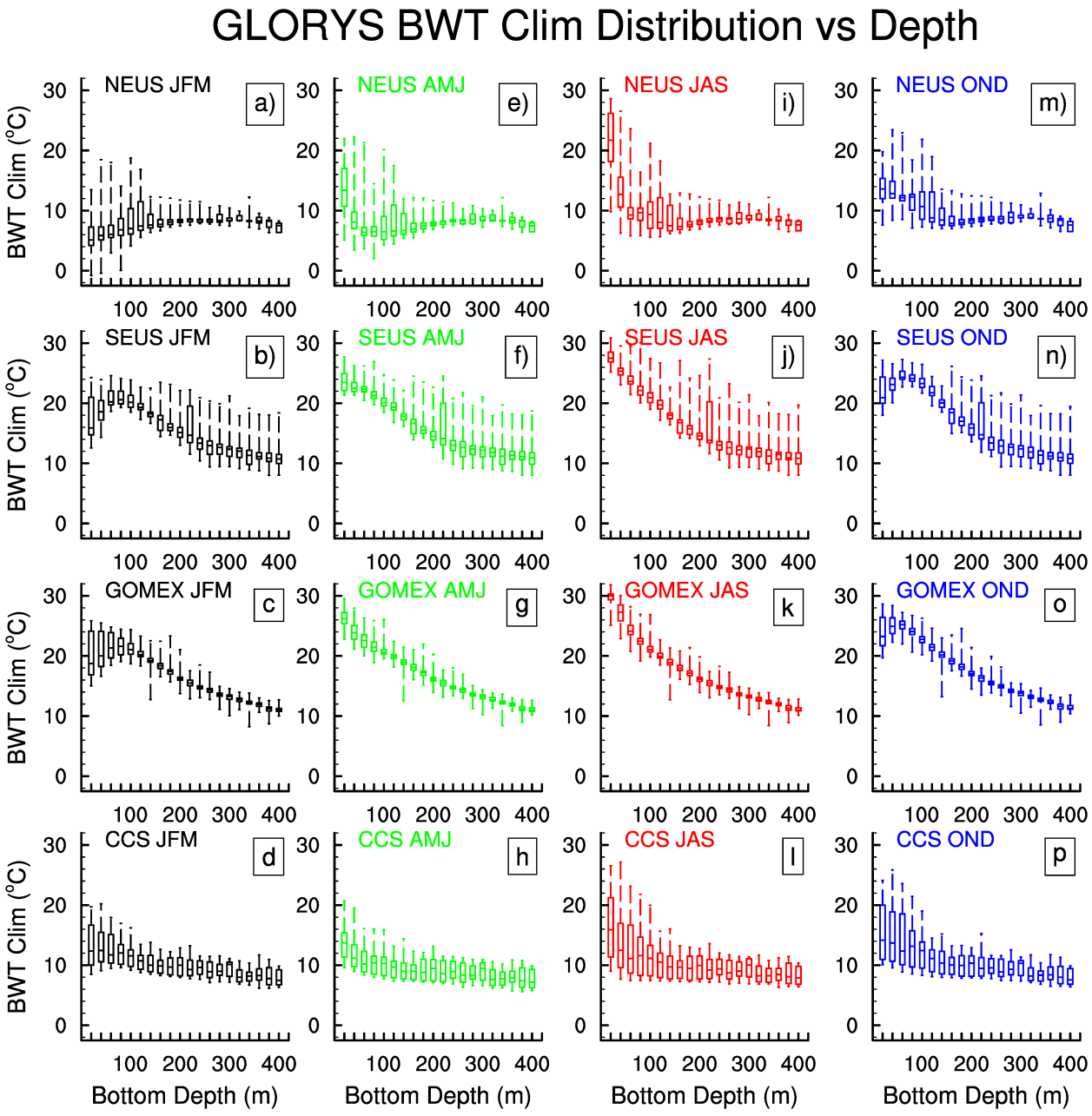

Fig. 4 BWT climatology as a function of bottom depth for coastal grid points < 400m deep. Grid points are separated by LME: (a,e,i,m) NEUS, (b,f,j,n) SEUS, (c,g,k,o) GOMEX, (d,h,l,p) CCS and season JFM (black), AMJ (green), JAS (red), OND (blue). Each “box and whisker” represents the distribution for a 20m range of depths. The ends of the whiskers are the max and min of the distribution and the ends of the boxes show the interquartile range, while the median is the midline of the box.

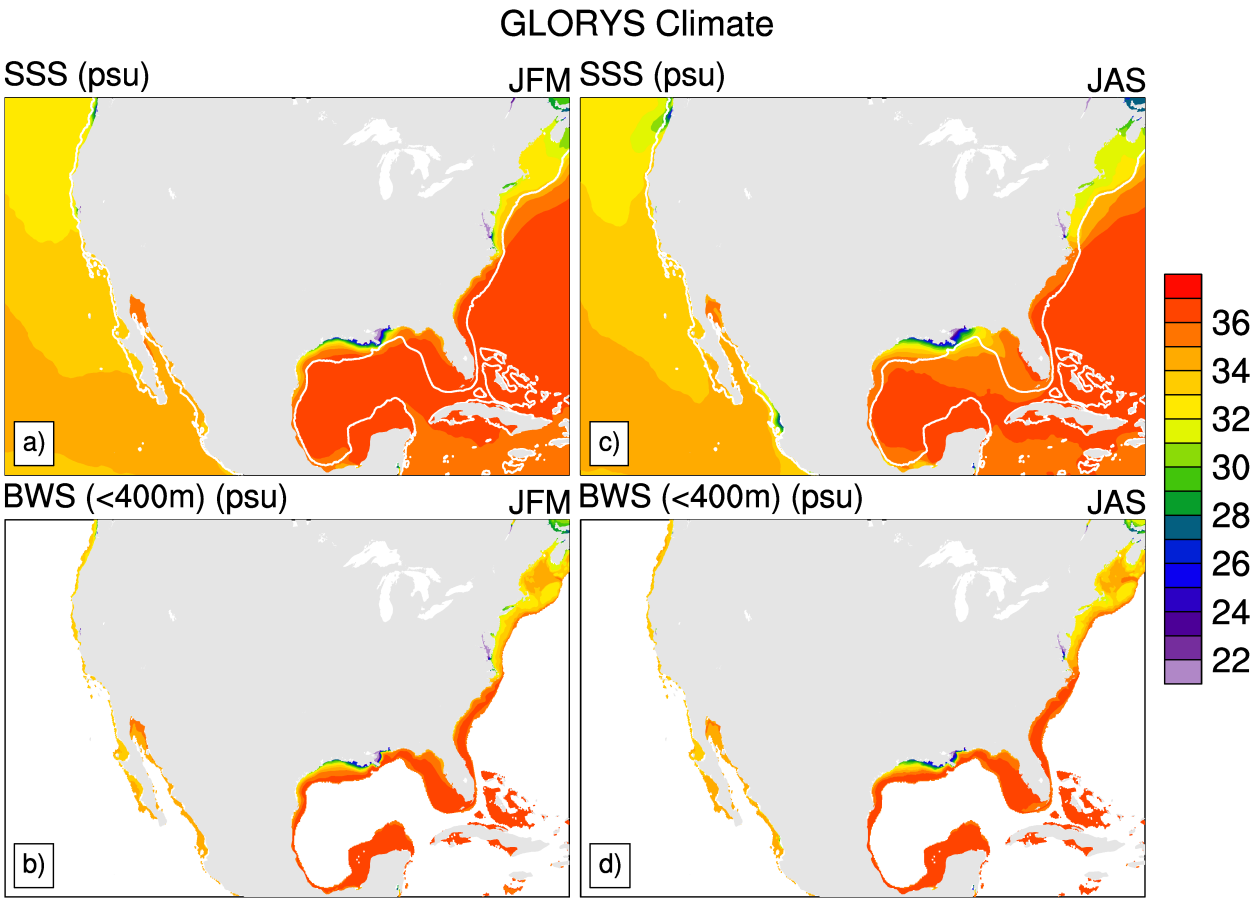

Fig. 5. Seasonal mean climate for (a,c) SSS and (b,d) BWS in JFM (left) and JAS (right). The 400m isobath (gray line) is shown in (a,c).

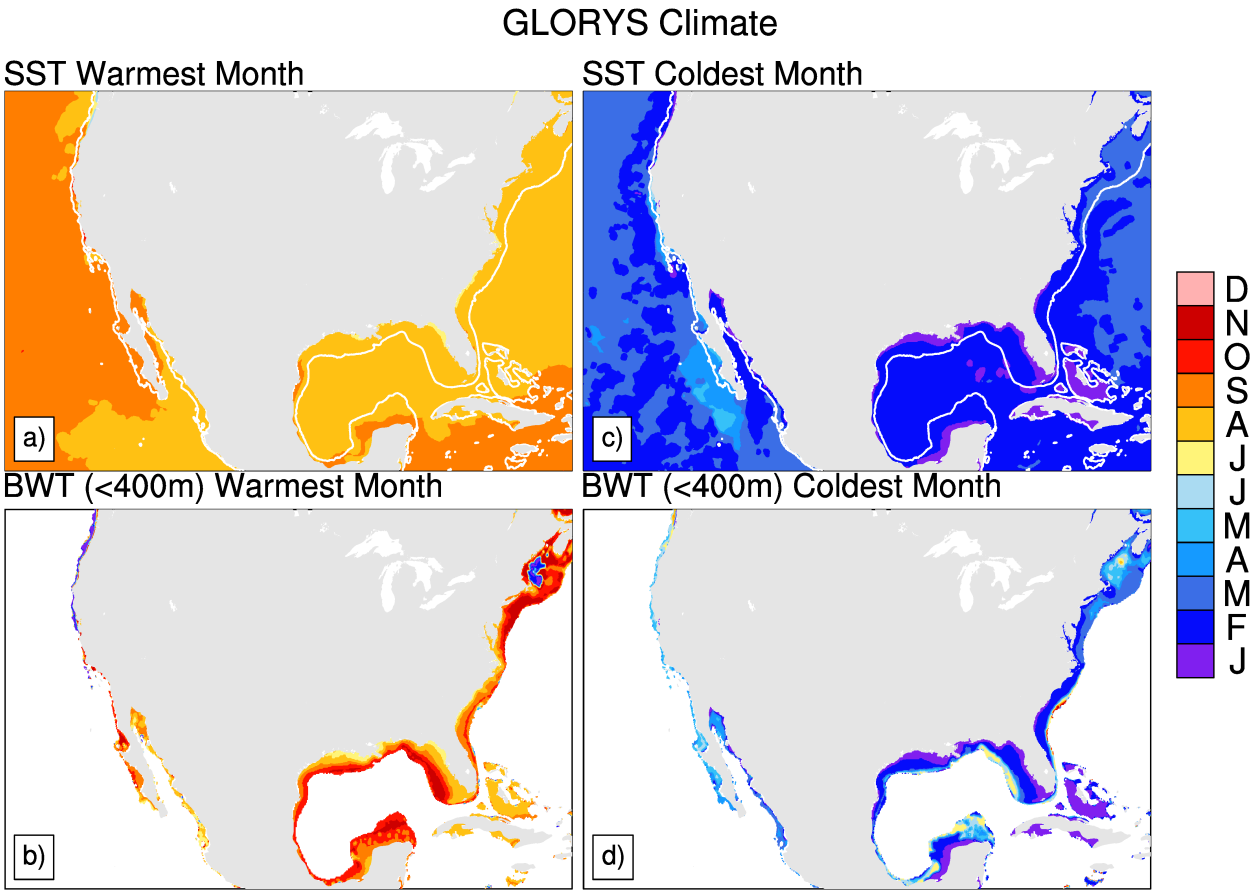

Fig. 6. Climatological warmest (left) and coldest (right) months in the seasonal cycle for (a,c) SST and (b,d) BWT. The 400m isobath (gray line) is shown in (a,c).

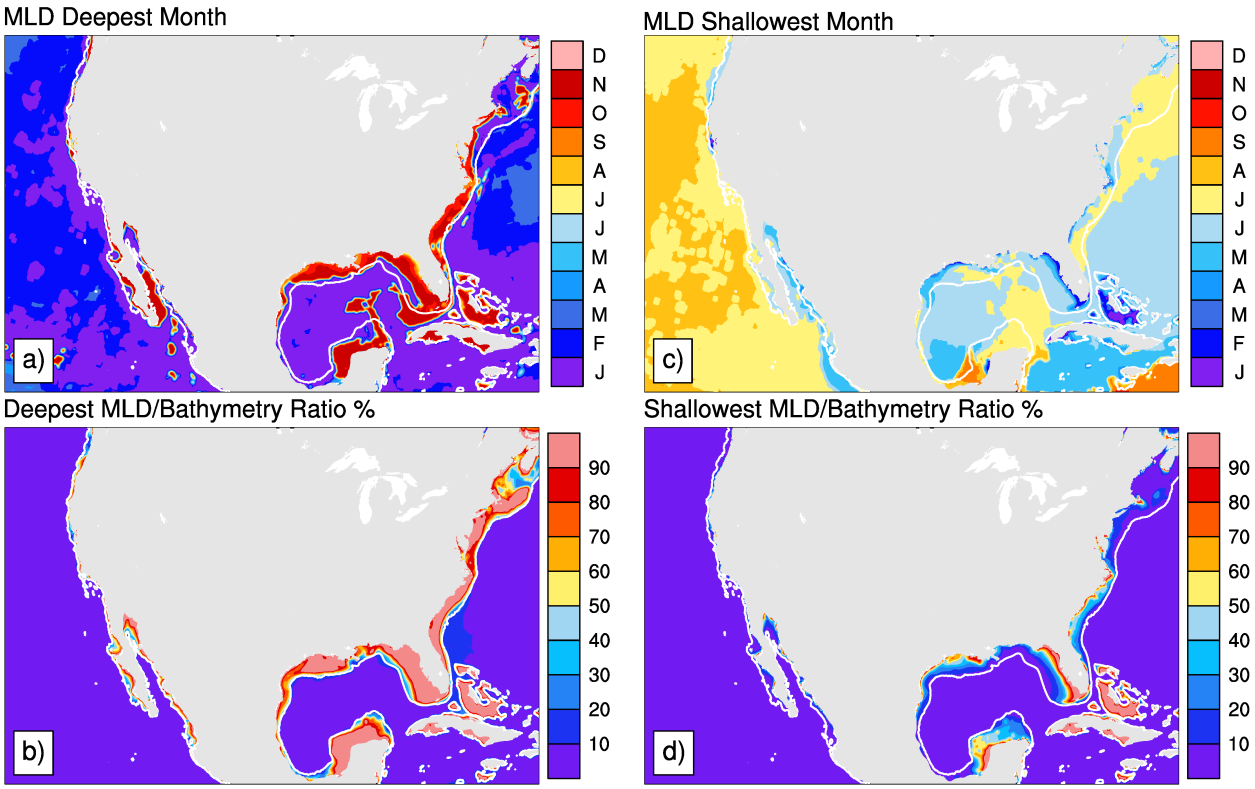

Fig. 7. Climatological deepest (left) and shallowest (right) months in the seasonal cycle for (a,c) MLD and (b,d) MLD as a percentage of the total column depth. The 400m isobath is shown by the gray line.

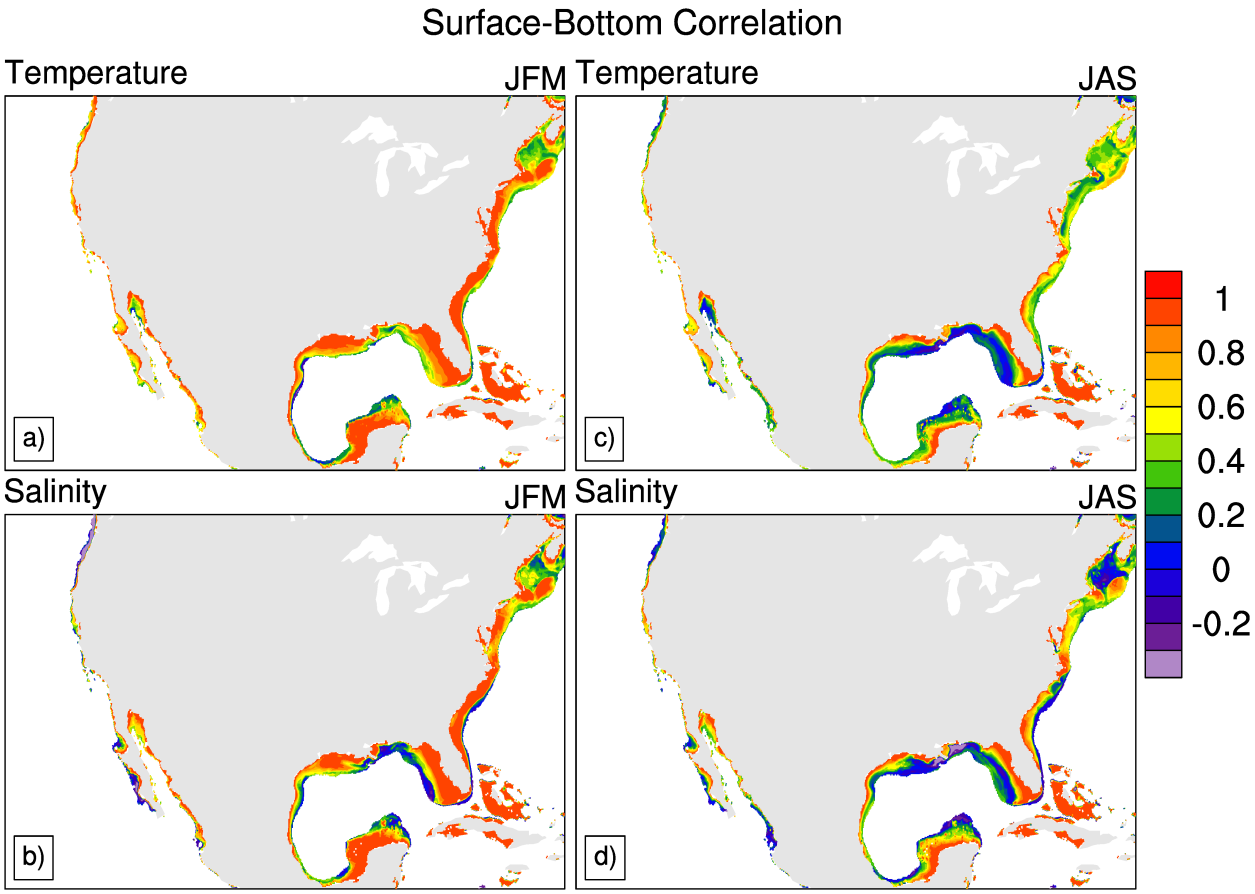

Fig. 8. Correlation of SST and BWT during (a) JFM and (b) JAS. Correlation of SSS and BWS during (c) JFM and (d) JAS.

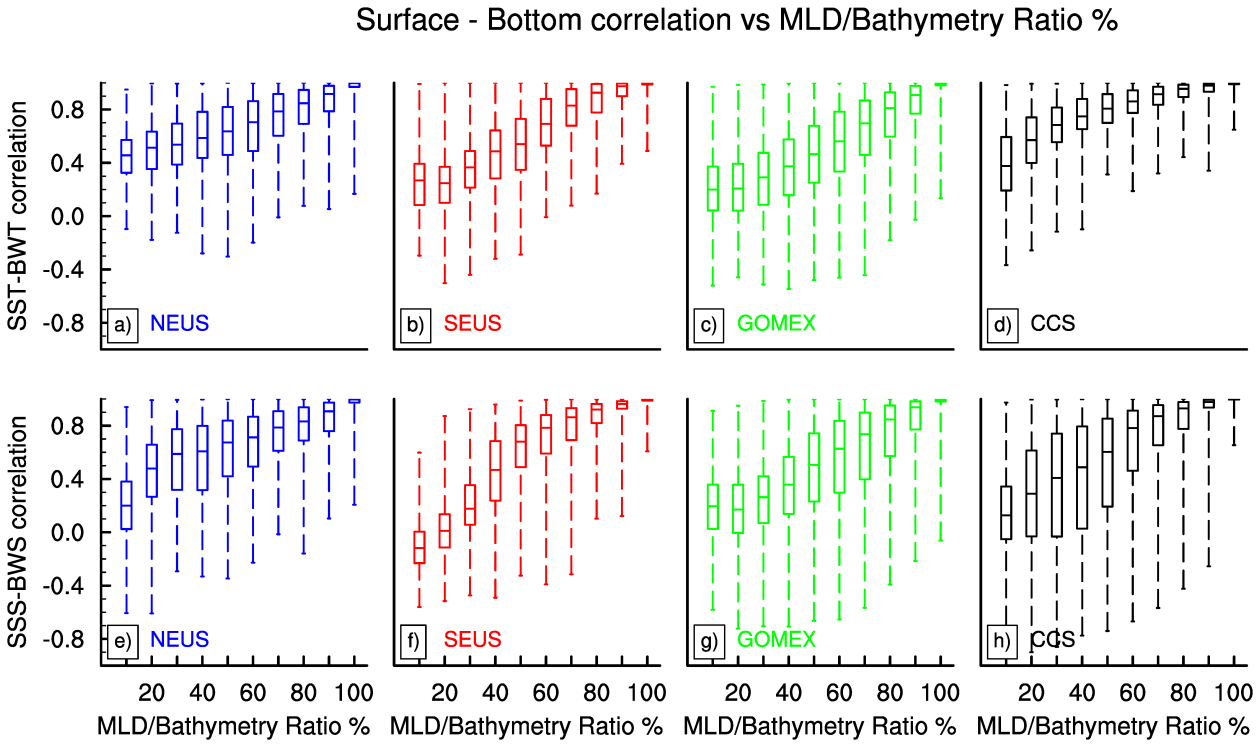

Fig. 9. Surface-Bottom correlations as a function of the mean mixed layer depth, as a percentage of total column depth for (a,b,c,d) temperature and (e,f,g,h) salinity, computed using monthly values aggregated over LME regions: (a,e) NEUS, (b,f) SEUS, (c,g) GOMEX and (d,h) CCS. The box and whiskers represent the spatial distribution of values within the LME in the MLD/bathymetry bin, where each bin represents 10% of the total column depth. The ends of the whiskers are the max and min of the distribution, the ends of the boxes show the interquartile range, and the median is the midline of the box.

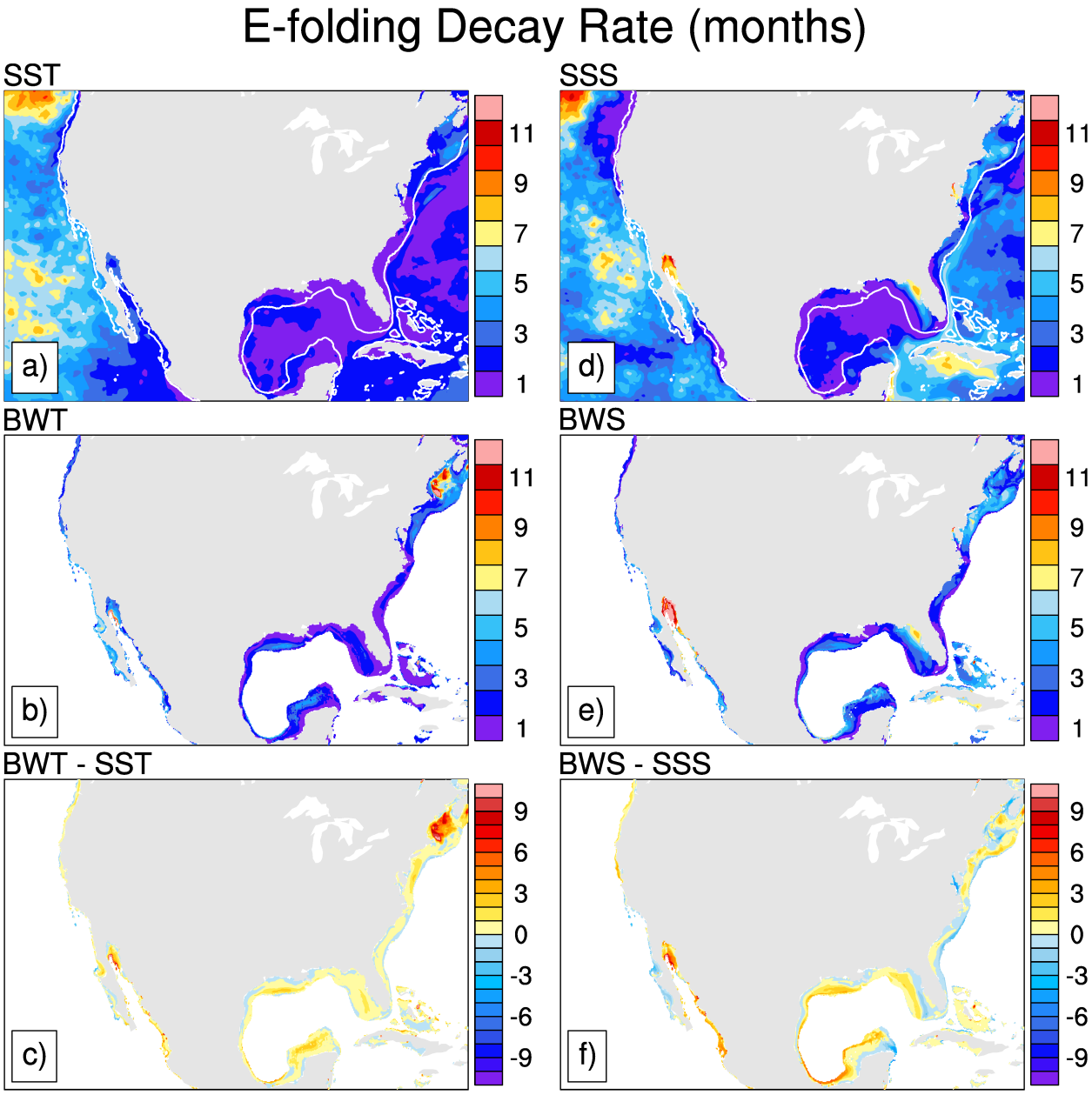

Fig. 10. Decay rate in months computed from autocorrelation at lags of 1 to 12 months (using the method described in Buckley et al., 2019) for (a) SST, (b) BWT, (c) BWT - SST, (d) SSS, (e) BWS, (f) BWS-SSS. The 400m isobath (gray line) is shown in (a,c).

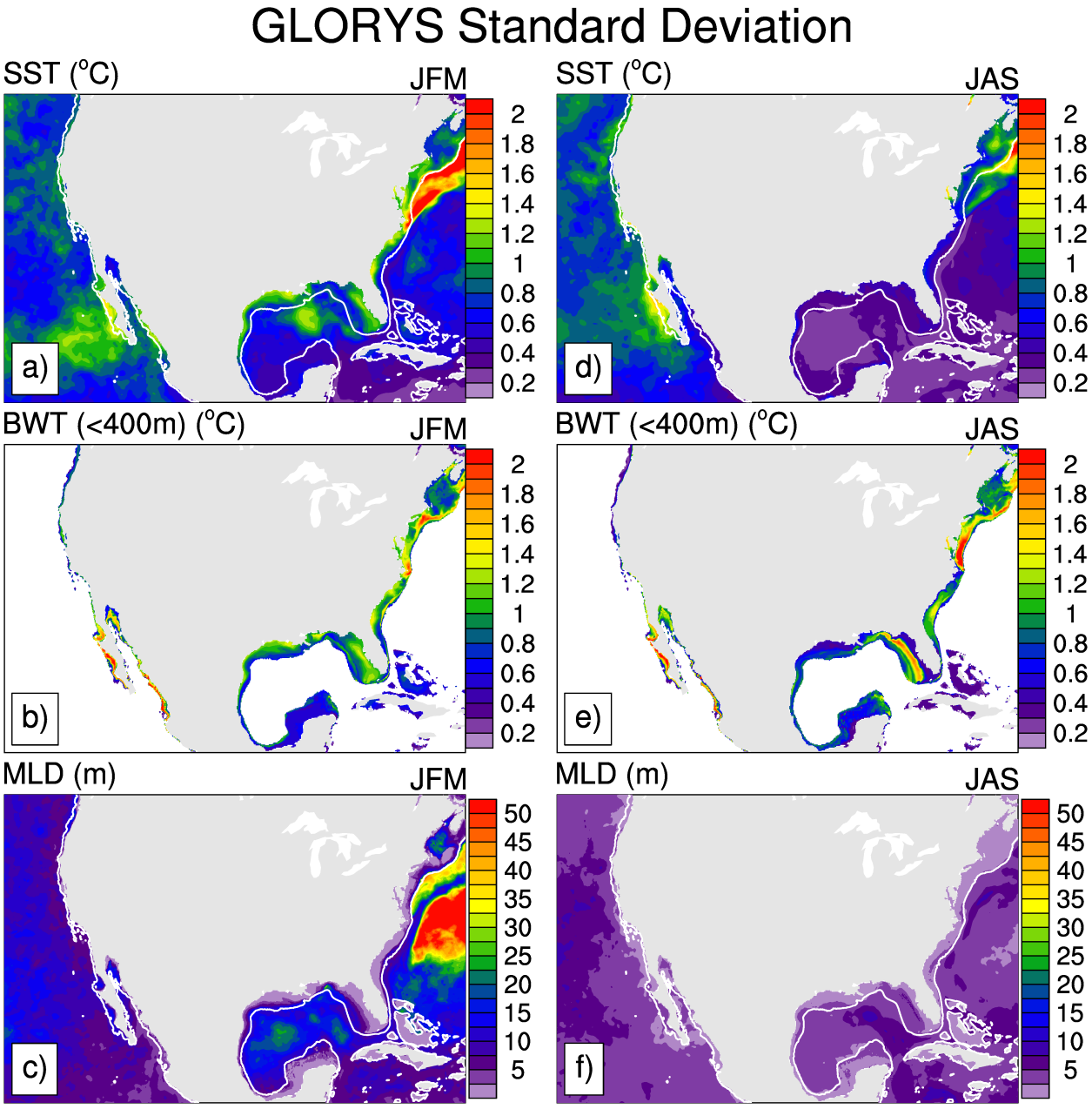

Fig. 11. Interannual Standard Deviation of (a,d) SST & (b,e) BWT (°C) and (c,f) MLD (m) for (left) JFM and (right) JAS. The 400m isobath (gray line) is shown in (a,c,d,f).

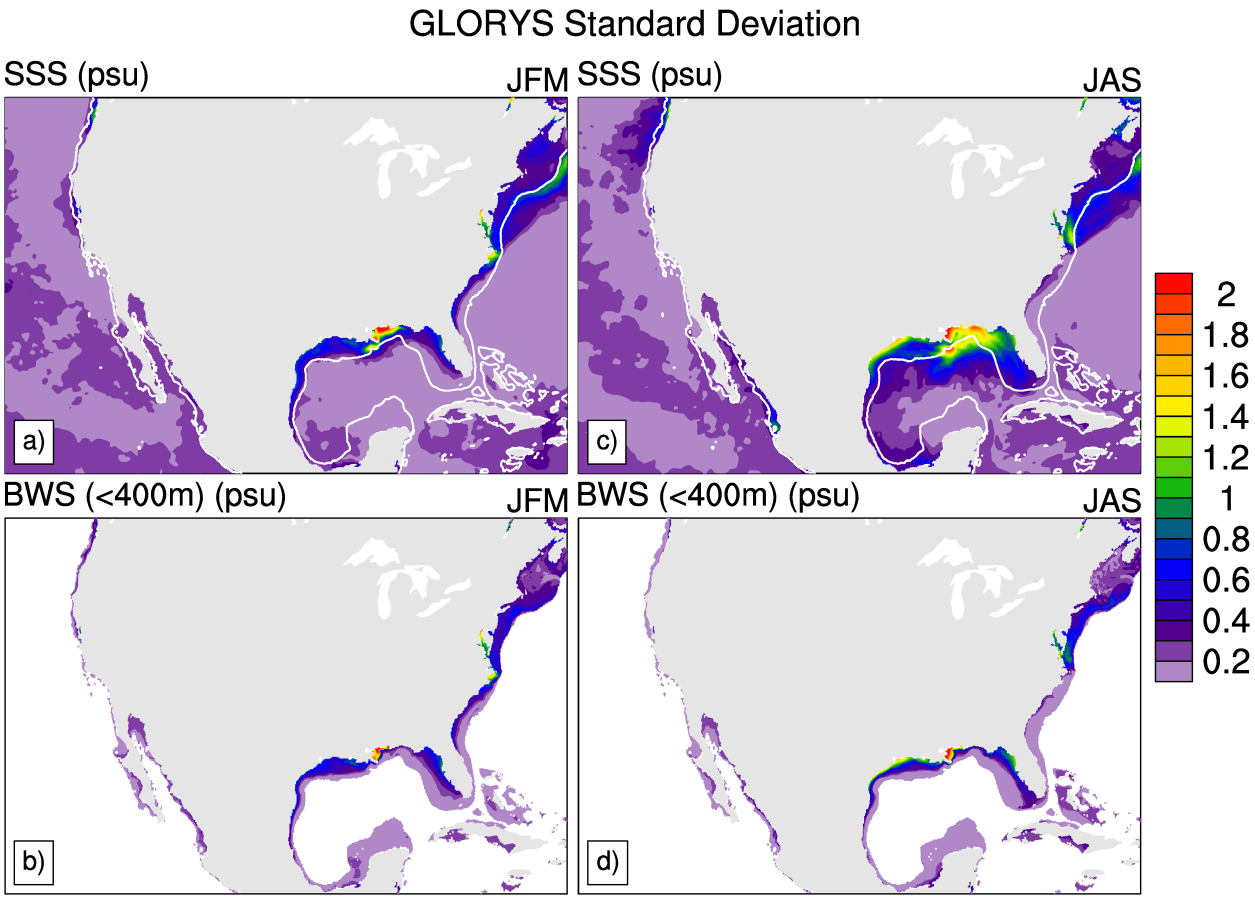

Fig. 12. Interannual standard deviation of (a,c) SSS and (b,d) BWS (psu) for (left) JFM and (right) JAS. The 400m isobath (gray line) is shown in (a,c).

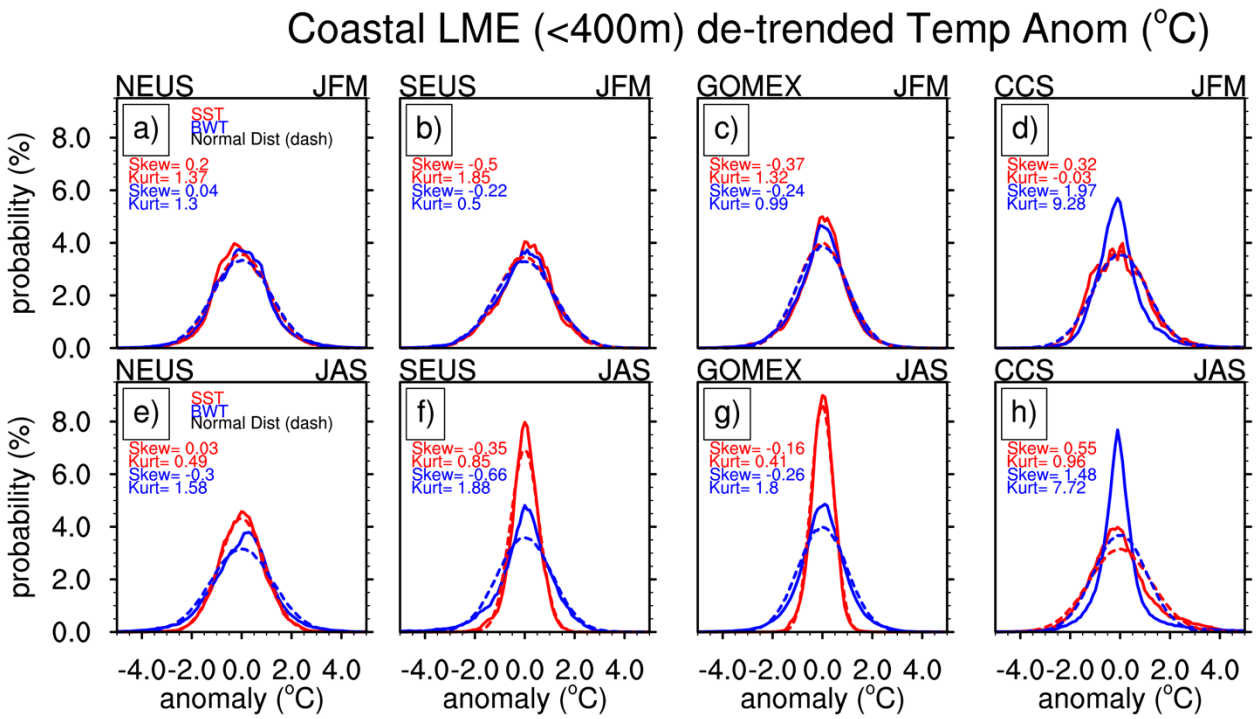

Fig 13. Probability distributions for all coastal points (< 400m) in each LME for SST (red) and BWT (blue) along with normal distributions (dashed lines) during (top) JFM and (bottom) JAS in (a,e) NEUS, (b,f) SEUS, (c,g) GOMEX and (d,h) CCS. Also shown are the skewness and kurtosis values. The skewness (third moment) measures the asymmetry. If the skewness > 0 (skewness <0), the tail of the distribution is longer on the right (left) side. The coefficient of kurtosis (fourth moment) measures the tails (outliers) of the distribution. The normal distribution has a kurtosis of 3, which is subtracted from the calculated kurtosis. If the calculated kurtosis > 0 (< 0), it is heavy (light) tailed with more (less) outliers, than a normal distribution.

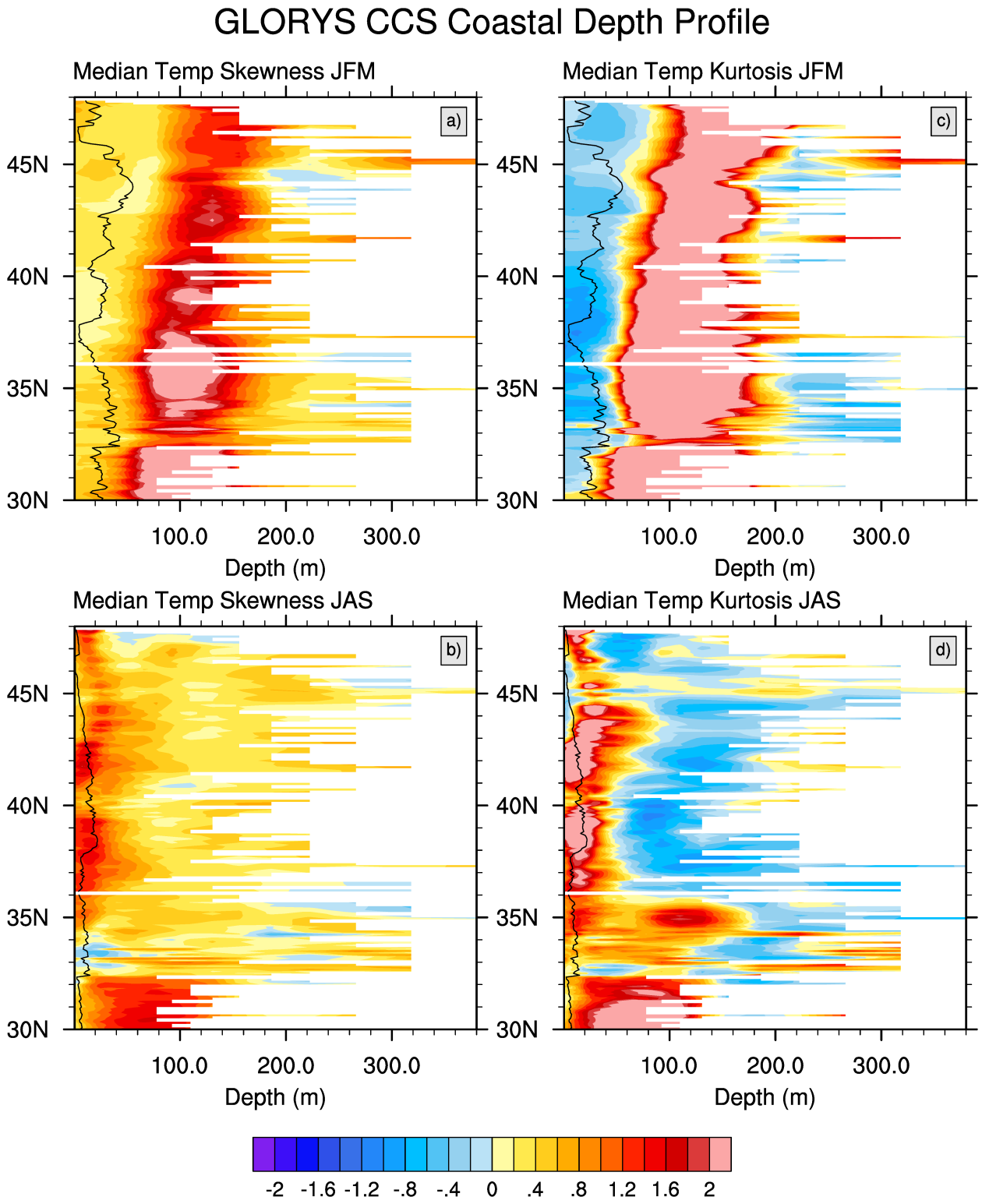

Fig 14. CCS LME median temperature (a,b) skewness and (c,d) kurtosis of monthly anomalies. Includes all longitude points shallower than 400 m at each latitude (from 30°N-48°N) over all depths in the column during (a,c) JFM and (b,d) JAS. Black contour indicates the median climatological MLD at each latitude.

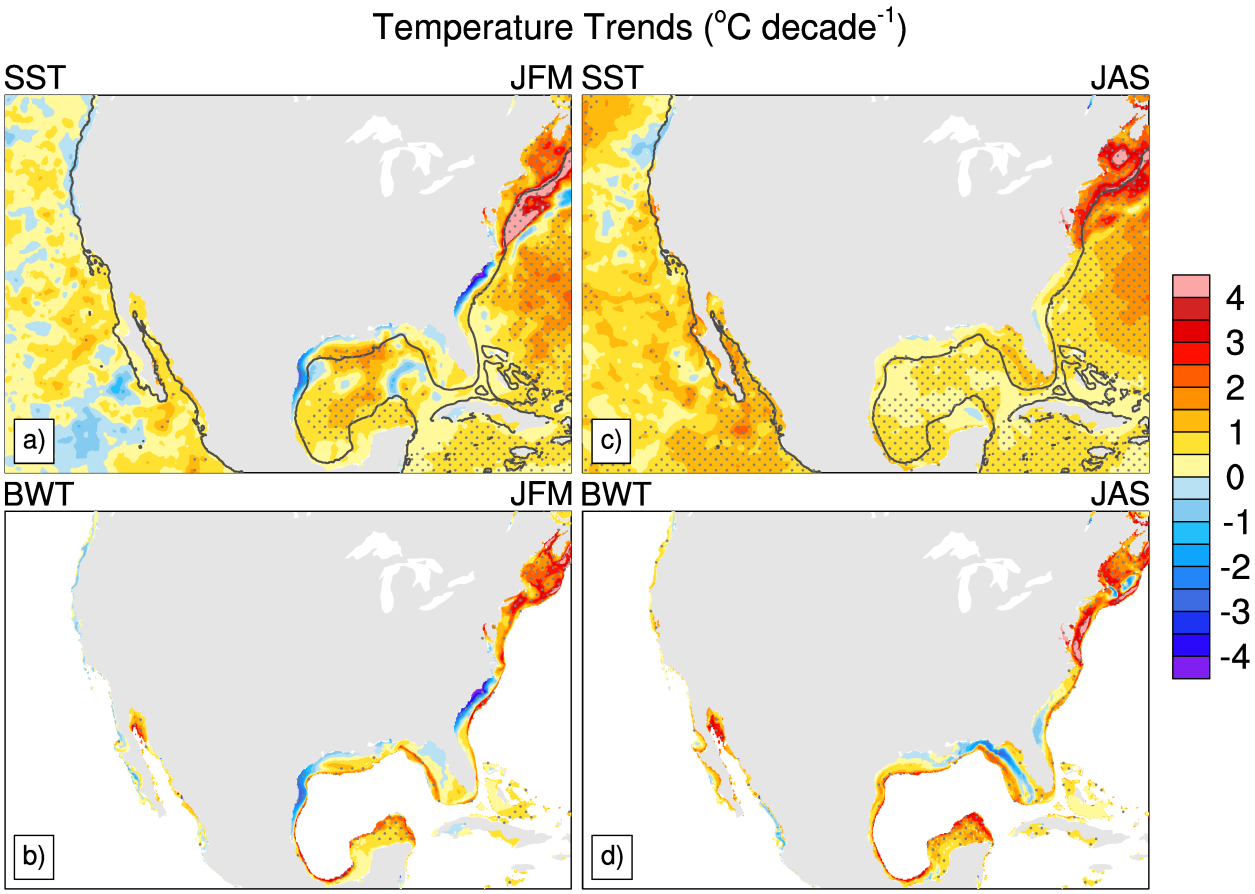

Fig. 15. Linear trends (f1993-2019) in (a,c) SST, and (b,d) BWT for (left) JFM and (right) JAS. Th 400m isobath (black line) is shown in (a,c). Significant trends (95%) using Mann-Kendall non-parametric test are indicated by stippling.

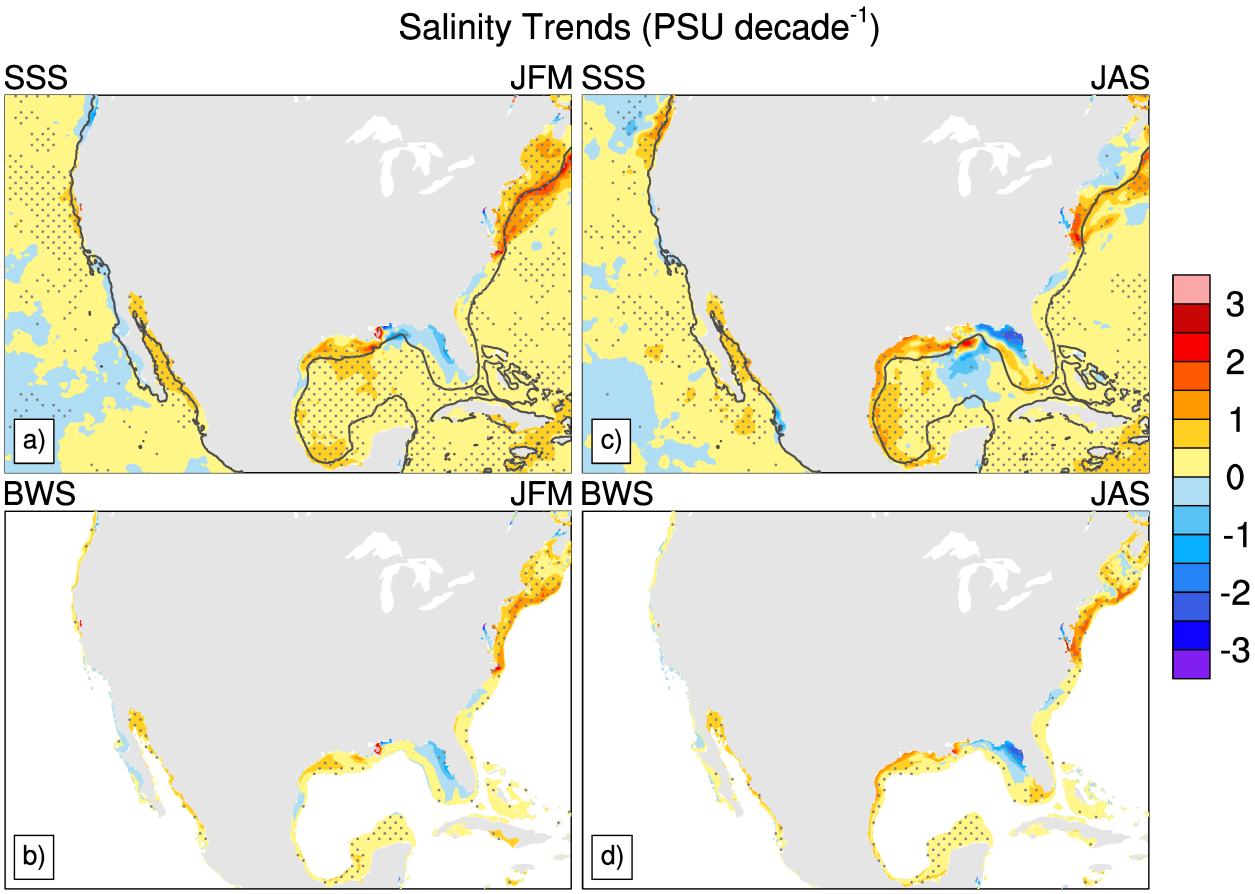

Fig. 16. As in Fig. 15 but for linear trends (1993-2019) in (a,c) SSS, and (b,d) BWS.

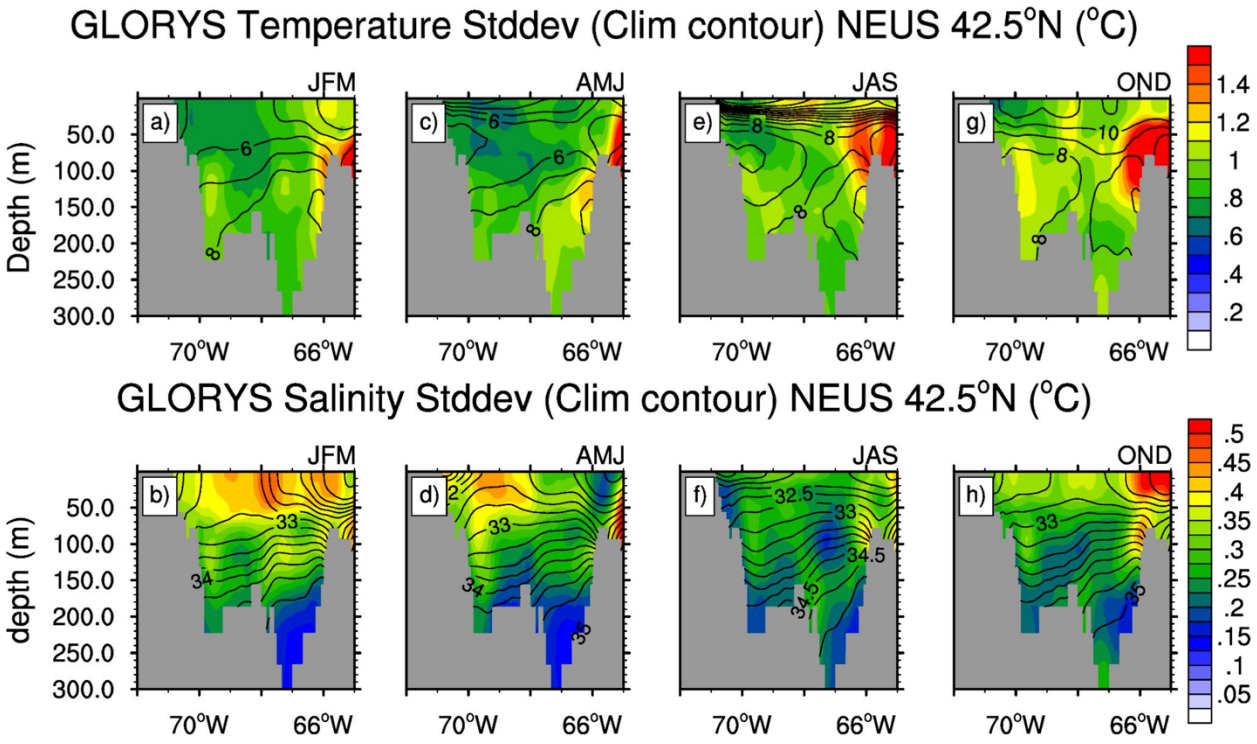

Fig. 17. Vertical cross-sections of (a,c,e,g) temperature (°C) and (b,d,f,h) salinity (psu) standard deviation (shading) and climatology (contours) along 42.5°N in the NEUS for (a,b) JFM, (c,d) AMJ, (e,f) JAS and (g,h) OND. Location of the cross section is shown as a gray line in Fig. 1.

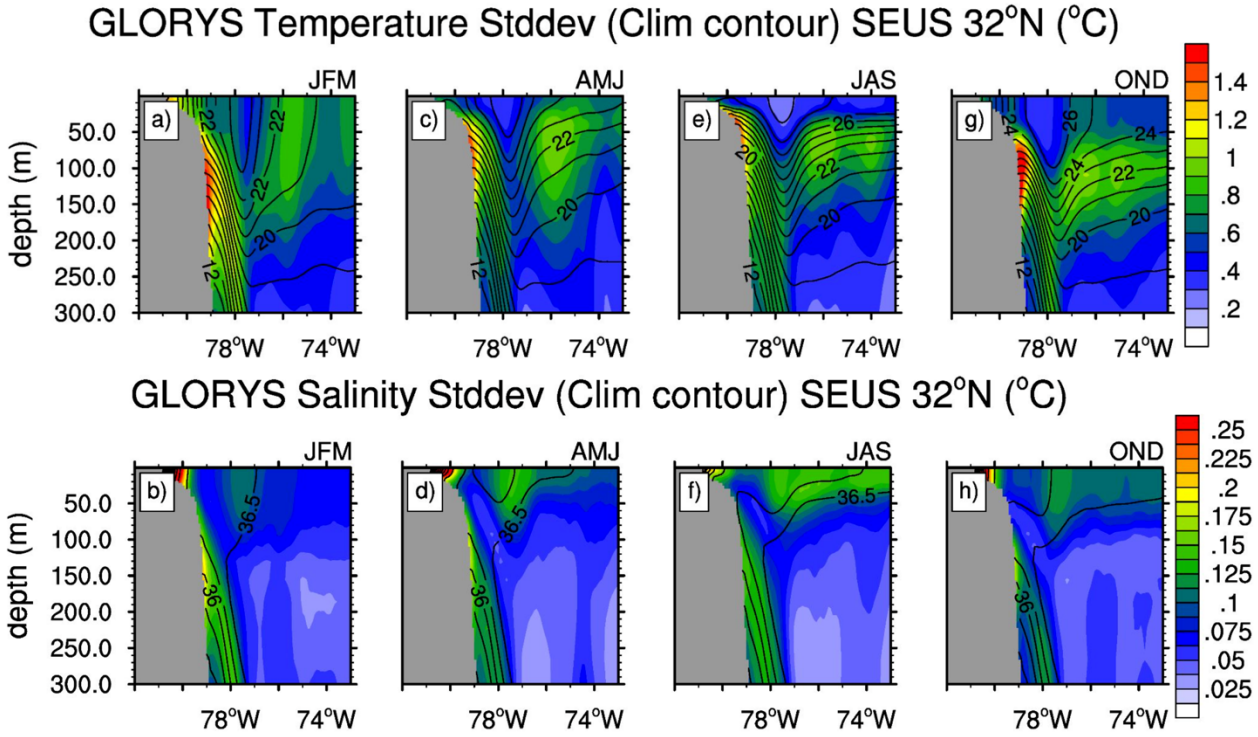

Fig. 18. As in Fig. 17 but for vertical cross-sections of temperature and salinity along 32°N in the SEUS.

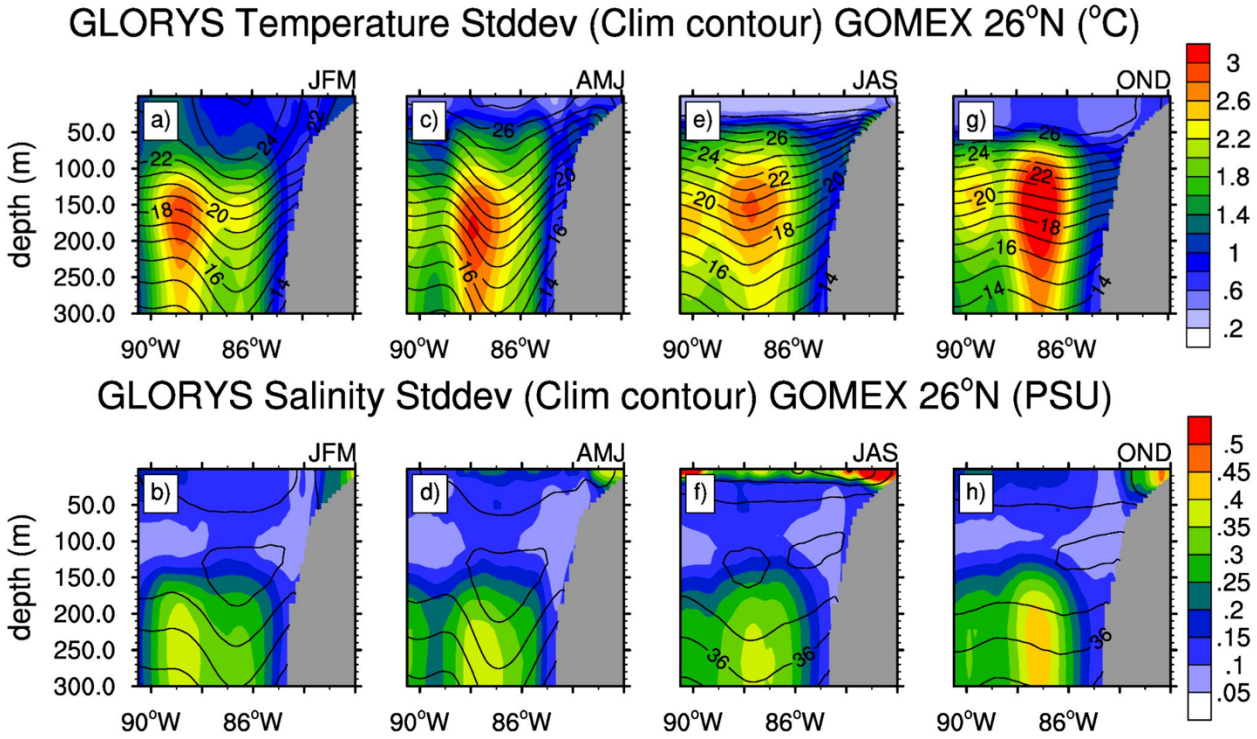

Fig. 19. As in Fig. 17 but for vertical cross-sections of temperature and salinity along 26°N in the GOMEX.

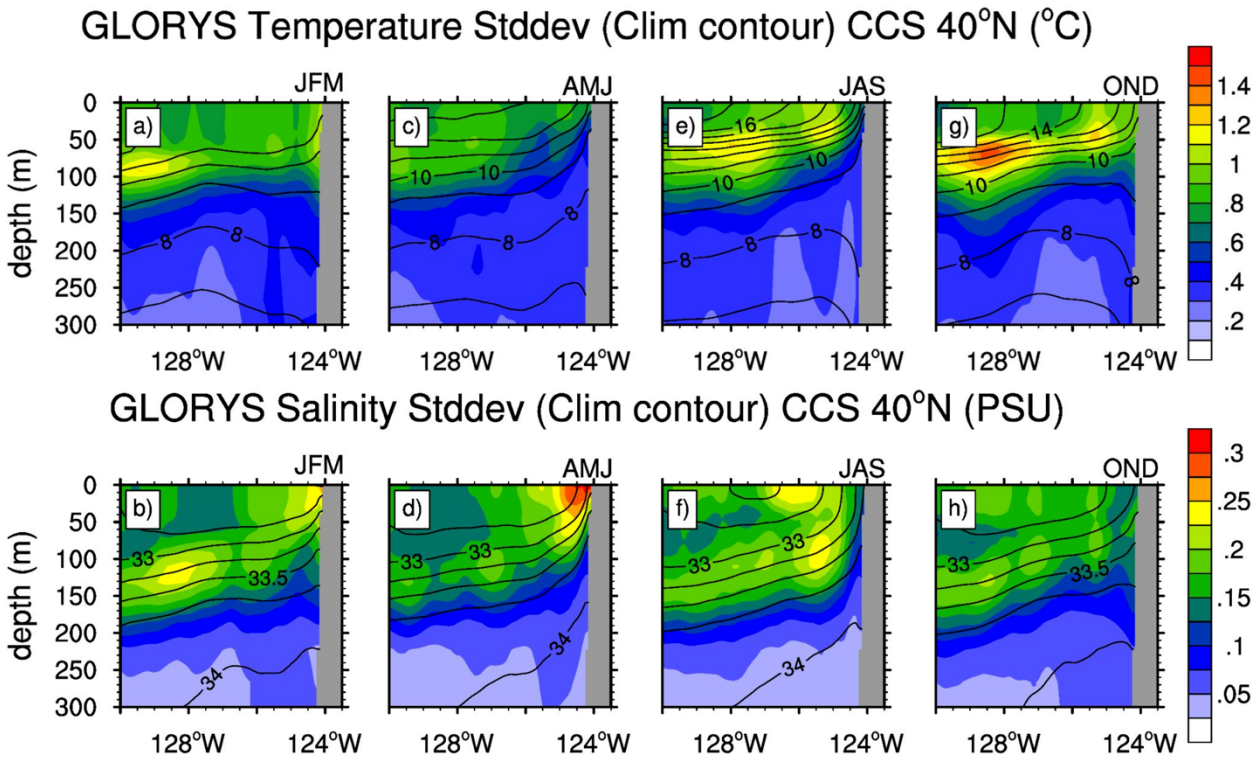

Fig. 20. As in Fig. 17 but for vertical cross-sections of temperature and salinity along 40°N in the CCS.